MSc Dissertation

ANALYSIS OF DYNAMICS OF BLADED DISCS WITH MONOCRYSTALLINE ANISOTROPIC BLADES

(Word Count: 11897)

A Thesis Submitted in Partial Fulfilment of the Requirement for the Award of the Degree of **Master of Science (MSc.)** in **Advanced Mechanical Engineering**

Submitted by

Candidate No: 153088

Under the Supervision and Guidance of

Dr. Evgeny Petrov

Reader in Structural Dynamics, Department of Engineering and Design

School of Engineering and Informatics, University of Sussex

Falmer, Brighton, UK

September - 2016

Disclaimer

University of Sussex MSc Advanced Mechanical Engineering project report

I certify that the attached dissertation is my own work except where otherwise indicated. I have referenced my sources of information; in particular I have placed quotation marks before and after any passages that have been quoted word-for-word, and identified their origins.

Dibakor Boruah Dated: 01/09/2016

Acknowledgements

I am pleased to acknowledge to all those who motivated, cooperated and helped me during the progress of my dissertation titled “Analysis of Dynamics of Bladed Discs with Monocrystalline Anisotropic Blades”. I am taking this opportunity to thank everyone who was associated with me during the project work.

I would like to offer my warm regards and humble thanks to Dr. Evgeny Petrov, School of Engineering & Informatics, University of Sussex for his valuable guidance, continuous support, help and advice.

I am very thankful to my classmates for their utmost help and suggestions towards the completion of my project work.

Finally, I would like to thank my parents and to all the people who encouraged me towards completion of my project work.

Abstract

The present study aims to quantify the effects of material anisotropic orientations on the dynamics of a gas turbine bladed disc with monocrystalline anisotropic blades (nickel-based superalloy DZ125). In consequence, a single blade finite element model has been created to analyse the effects of material anisotropy on the modal properties of a single blade of a gas turbine. Then, a finite element sector model with cyclic symmetry has been generated to analyse the influence of anisotropic material orientations on the natural frequency and mode shapes of a tuned bladed disc. Moreover, a whole bladed disc finite element model (tuned and mistuned) has been created to investigate the effects of anisotropic material orientations on the forced responses of a mistuned bladed disc of a gas turbine. Finally, results have been analysed to evaluate the variation of the natural frequency of a single blade and a tuned bladed disc respectively caused by the variation of anisotropic orientations of the blade material. Also, normalised forced responses of the mistuned bladed disc with four different mistuning patterns have been analysed against a number of blades of the whole bladed disc.

The outcome of these analyses indicates that the material anisotropy has a significant effect on the dynamic properties of a gas turbine bladed disc. In the case of a single blade, maximum frequency variation due to material anisotropy is found to be 5.3 % among the analysed cases. For tuned bladed disc, maximum frequency variation is found to be 5.1 % amongst the examined cases. Also, a discussion has been accomplished in terms of how Eulerian angles (primary and secondary angles) affects the natural frequency variations for different analysed cases of anisotropic orientations. Furthermore, amplification factor or normalised maximum forced responses are found to be within the range of 0.66 to 1.85 for the investigated cases of mistuned bladed disc with monocrystalline anisotropic blade material.

Contents

List of Figures

List of Tables

List of Symbols

E	Young's modulus
G	Shear modulus
ν	Poisson's ratio
ρ	Density
ε_x	Normal stress
σ	Shear strains
φ	Primary angle (rotation angle about the [100] axis)
θ	Primary angle (rotation angle about the [010] axis)
Ψ	Secondary angle
K	Stiffness matrix
M	Mass matrix
ϕ_j	j^{th} mode shape
ω_j	j^{th} natural frequency
C	Damping matrix
q	Vector of nodal displacements
f	Vector of excitation nodal forces.
F	Complex amplitudes of excitation forces
Q	Vector of complex amplitudes of displacements.
$\Delta\Omega$	Frequency interval
N	Total number of blades in the bladed disc
k	Engine order
j	Blade number

Chapter 1

Introduction

1.1 General overview

In the current scenario, gas turbines play a vital role in the field of power generation. Gas turbine blades are one of the chief components of a turbine, but then again it accounts for utmost failures happening in the gas turbines. Hence, there is a demanding necessity for the analysis of different aspects affecting the performance of blades. The blades of a turbine play a major role when determining the life and overall efficiency of a gas turbine. The turbine blades are exposed to various forces, principally centrifugal due to rotating motion, and bending loads owing to fluid pressure & change of momentum [1].

Since, gas turbine blades are operating at very high temperatures, therefore turbine blades always experience heating and cooling transients during the period of start-up and shutdown. Failure of turbine blades are mainly due to complex loadings, comprising low cycle fatigue, thermo-mechanical fatigue, creep, creep–fatigue interaction, etc. In order to achieve required material properties, modern turbine blades are every so often manufactured by using directional solidification process [2]. Directional solidification results in the high anisotropy of the material properties. Due to inevitable scatter in the anisotropic properties of blades, bladed discs of gas-turbine engines are mistuned. Generally mistuning is unavoidable in nature, mistuning can lead to a dramatic growth in blade stresses and forced-response amplitudes excited in bladed discs by the gas flow, even a small amount of mistuning may lead to a huge variation in the blades' forced response amplitudes by a factor of 2 or more in many cases [3-11].

This study comprises of evaluating the effect of material anisotropy on the modal properties, natural frequencies and forced responses of a bladed discs mistuned by blade material anisotropy. The studies

of mistuning effects have been performed using finite element models of bladed discs generated in ANSYS.

1.2 Objectives

The major objectives of this study are to evaluate the effects of material anisotropy on natural frequencies, modal properties of a single blade of a gas turbine and a tuned bladed disc. Moreover, to evaluate the material anisotropy effects on the forced response of a mistuned bladed disc. Therefore, the three principal objectives of this study are as follows:

1) Analysis of material anisotropy effects on natural frequencies and mode shape of a single gas turbine blade.
2) Analysis of anisotropy orientation effects on the natural frequencies and modal properties of a tuned bladed disc of a gas turbine.
3) Analysis of modal characteristics and forced response of bladed discs of a gas turbine with mistuning due to anisotropy orientation scatters.

1.3 Introduction to the fundamentals

A brief description of the fundamental subjects associated with the current study is presented in this section, which includes the process of Directional Solidification of gas turbine blades, Anisotropic Materials, Mistuned Bladed Discs, Finite Element Analysis, Modal Analysis and Forced Response Analysis.

1.3.1 Directional solidification

Directional solidification defines a process of solidification which takes place from the farthest end of the casting and works its way towards the sprue [12]. It refers to the process of producing a casting by feeding of the molten metal in a controlled manner into a temperature-controlled mould to produce a part, which is free from internal cavities and voids or shrinkage defects. Also, the directional solidification technique is used to refine the metal during the casting process [13].

During the process of directional solidification, the molten metal at the far end of the mould starts to cool and solidify before the rest of the mould cools and solidify. As soon as the metal cools on the bottom of the mould, the solidification line moves gradually upward toward the molten metal feed. By introducing thermal variations in the mould and controlling the rate of flow of the molten metal feed, shrink defects of can be removed, since the liquid metal flows naturally into the dips and vacant areas.

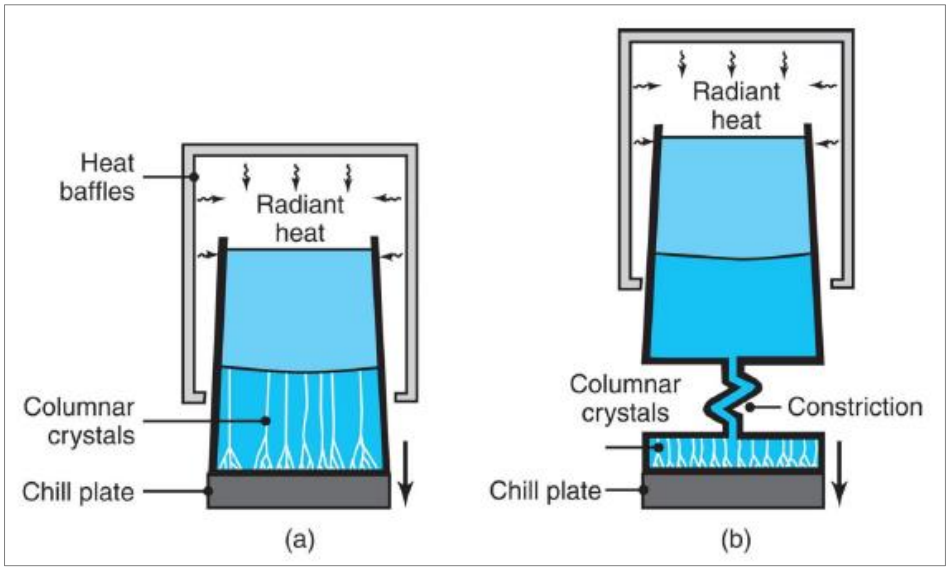

Figure 1: (a) Directional Solidification, and (b) Method to produce single crystal blade [14]

Figure 1 shows manufacturing process of a gas turbine blade with directional solidification and method to produce single crystal blade [14].

Directional solidification results in the high anisotropy of the material properties. A brief description of the anisotropic material is given below.

1.3.2 Anisotropic materials

The anisotropic material exhibits different mechanical, elastic and thermal properties (elasticity moduli, shear moduli, Poisson's ratios, heat conductivity, etc.) in different directions based on the spatial orientation of the physical body, for example: wood and composites [15]. Several materials are anisotropic and inhomogeneous because of their variable composition of their constituents. Among the range of anisotropic construction materials, of the greatest practical value are the so-called

orthotropic and transversally isotropic materials [16]. A brief description of the orthotropic materials is given below.

Orthotropic materials

The orthotropic material is a type of the anisotropic material. Orthotropic materials possess three mutually orthogonal planes of elastic symmetry, along which its properties remain constant. Orthotropic materials include various crystals and composite materials with a regular structure. By convention, in orthotropic constitutive equations, the 9 elastic constants are comprises of 3 Young's moduli (E_x, E_y, E_z), 3 shear moduli (G_{yz}, G_{zx}, G_{xy}), and 3 Poisson's ratios (ν_{yz}, ν_{zx}, ν_{xy}). In case of orthotropic materials, there is no interaction between the normal stresses $(\varepsilon_x, \varepsilon_y, \varepsilon_z)$ and the shear strains $(\sigma_{yz}, \sigma_{zx}, \sigma_{xy})$, the matrix form of the Hook's law can be represent as follows [16, 17].

$$\begin{bmatrix} \varepsilon_{xx} \\ \varepsilon_{yy} \\ \varepsilon_{zz} \\ \varepsilon_{yz} \\ \varepsilon_{zx} \\ \varepsilon_{xy} \end{bmatrix} = \begin{bmatrix} \frac{1}{E_x} & -\frac{\nu_{yx}}{E_y} & -\frac{\nu_{zx}}{E_z} & 0 & 0 & 0 \\ -\frac{\nu_{xy}}{E_x} & \frac{1}{E_y} & -\frac{\nu_{zy}}{E_z} & 0 & 0 & 0 \\ -\frac{\nu_{xz}}{E_x} & -\frac{\nu_{yz}}{E_y} & \frac{1}{E_z} & 0 & 0 & 0 \\ 0 & 0 & 0 & \frac{1}{2G_{yz}} & 0 & 0 \\ 0 & 0 & 0 & 0 & \frac{1}{2G_{zx}} & 0 \\ 0 & 0 & 0 & 0 & 0 & \frac{1}{2G_{xy}} \end{bmatrix} \begin{bmatrix} \sigma_{xx} \\ \sigma_{yy} \\ \sigma_{zz} \\ \sigma_{yz} \\ \sigma_{zx} \\ \sigma_{xy} \end{bmatrix} \quad \text{…….. (1)}$$

Where, $\frac{\nu_{yz}}{E_y} = \frac{\nu_{zy}}{E_z}$, $\frac{\nu_{zx}}{E_z} = \frac{\nu_{xz}}{E_x}$, $\frac{\nu_{xy}}{E_x} = \frac{\nu_{yx}}{E_y}$

1.3.3 Crystallographic orientations

Single-crystal superalloys possess highly orthotropic material characteristics that differ significantly with direction relative to the crystal lattice. During casting process monocrystalline nickel-based turbine blades are directionally solidified with the crystallographic direction [001] aligned with the stacking axis of the blade. Owing to casting inconsistency, a perfect alignment of the [001] or primary

axis is not possible in practical cases. As shown in Figure 2, the airfoil stacking axis is usually controlled within the range of 0° to 15° relative to the crystallographic direction [001], known as a Primary angle. The position of primary angle is defined by two angles 'φ' and 'θ', as can be seen in the Figure 3; where, angle φ defines rotation angle about the [100] axis (Z axis), whereas angle θ designates rotation angle about the [010] axis (X′).

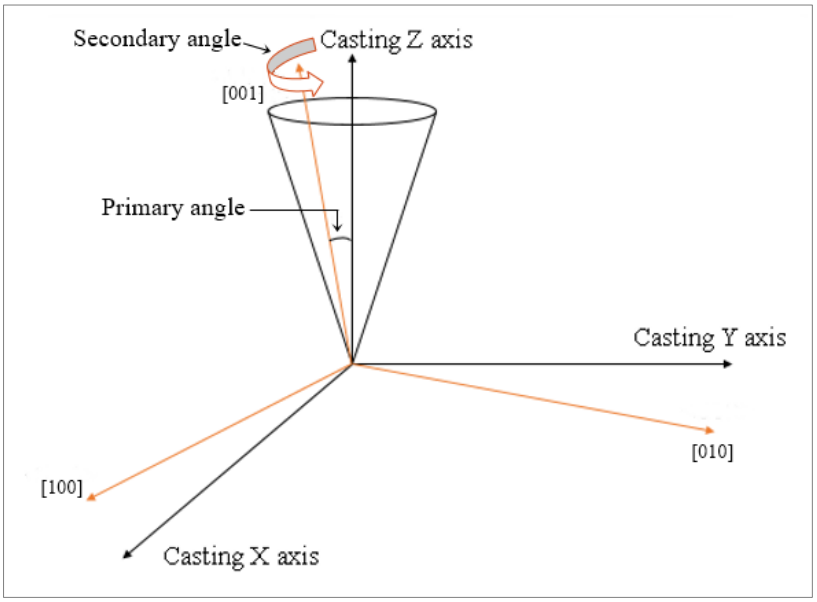

Figure 2: Orientation of primary axis with regard to the blade stacking axis

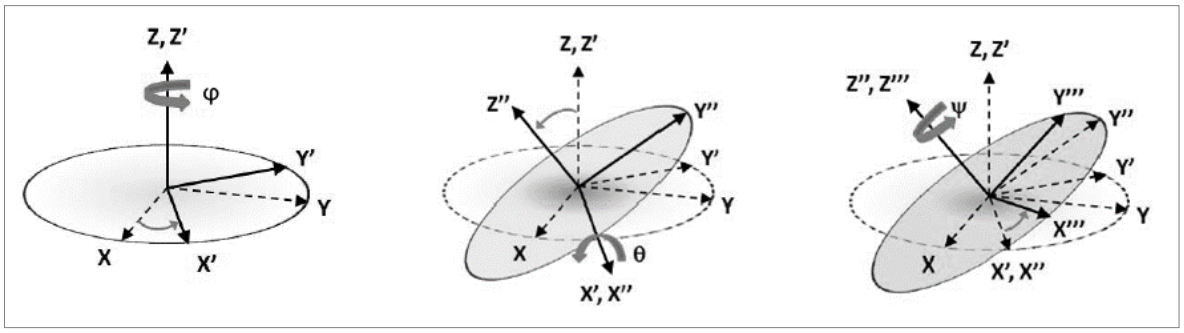

Figure 3: Eulerian angles involving three rotation [18]

In most of the turbine blade casting, the rotation of the single crystal about the primary axis is generally neither specified nor controlled, which is known as Secondary angle 'Ψ'. Secondary angle (Ψ) is the third rotation about the [001] axis (Z″ axis). The angle Ψ is an arbitrary variable for a single crystal turbine blade. However, Ψ angle for each blade is usually recorded after the casting process is

complete. Since, each blade can have a different secondary orientation, finite element analysis of the blades has to account for a range Ψ orientations between 0 ° and 90° [18, 19, 20].

1.3.4 Mistuned bladed discs

Due to inevitable scatter in the anisotropic properties of blades, bladed discs of the gas-turbine engines are mistuned. Mistuning denotes the variations in modal properties of blades caused by the anisotropic material orientation of anisotropic turbine blades and due to slight differences in their geometries that arise thru the manufacturing and assembly procedure. Generally mistuning is unavoidable in nature; even though a bladed disk is generally designed to have identical blades with same dimensions and of the same material, there are always random deviations among the blades caused by directional solidification process of single crystal blades, manufacturing tolerances, wear, and other causes. Mistuning may lead to a dramatic increase in blade stresses and forced-response amplitudes excited in bladed discs by the gas flow, even a small amount of mistuning may lead to a huge variation in the blades amplitudes by a factor of 2 or more in many cases [6-14].

1.3.5 Finite element analysis (FEA)

Finite element analysis is a computer based numerical method to analyse structures, fluid, magnetic, temperature fields etc., which allows modelling of loading conditions and geometry of a structure and determining its response to those conditions. In FEA, a structure is fragmented into an assembly of finite elements. These element sizes are selected to be small enough to allow lower-order polynomial approximations of the fields to be analysed (displacements, strains, stresses, etc.) through their values at a set of selected points. These approximations are applied to obtain relationships between nodal displacements and forces for each finite element in the form of a matrix. All finite element matrices are united to form and solve the finite element equation with respect to the nodal values & nodal degrees of freedom for the whole structure.

The main benefits of FEA are that it is one of the most reliable and appropriate analysis tool which allows effective analysis for a wide class of problems for structures of complex geometry, loading and material properties [21, 22].

1.3.5.1 Modal analysis

In structural dynamics, modal analysis is the field of measuring and analysing the dynamic response or properties of structures during vibrational excitation. The modal analysis in ANSYS is a linear analysis. The objective of the modal analysis is to determine the natural mode shapes and natural frequencies of an object during free vibration of a structure. The natural frequencies and natural mode shapes are important parameters in the design of a structure for dynamic loading conditions, in spectrum analysis or a mode superposition harmonic or transient analysis. Modal properties namely natural frequencies and mode shapes are dynamic properties of the structure reliant on structure geometry, material elastic properties, density and boundary conditions. The total number of mode shapes and natural frequencies is equal to the total number of degrees of freedoms (DOFs) in the model. The natural frequencies and mode shapes of an eigenproblem can be represented by the formula as given below-

$$K\phi_j = \omega_j^2 M\phi_j \qquad \text{..... (2)}$$

Where, K = stiffness, M = mass matrix, ϕ_j = j^{th} mode shape, ω_j = j^{th} natural frequency.

There are many mathematical methods to solve the eigenproblem in ANSYS viz. Block Lanczos, Reduced, Unsymmetric, Damped, QR Damped, PCG (Preconditioned Conjugate Gradient) Lanczos, and Supernode [23].

1.3.5.2 Harmonic forced response analysis

In a structural system, any sustained cyclic load produces a sustained cyclic or harmonic response. Harmonic response analyses are used to determine the steady-state, forced response of a linear structure to loads which vary sinusoidally or harmonically with time, which enables to confirm whether the designs will successfully overcome fatigue, resonance and other destructive effects of forced vibrations or not [24, 25].

Harmonic analysis is a linear analysis that calculates structure's response at a number of frequencies and obtains a graph of some response quantity (generally displacements) versus frequency. Peak responses are then recognised on the graph and stresses reviewed at those peak frequencies.

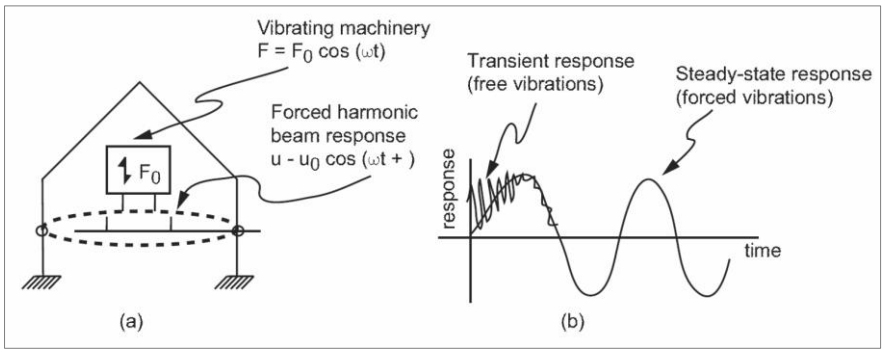

Figure 4: a) A typical harmonic response system; b) A transient and steady-state dynamic response [24]

The equation of motion of a vibrating structure is generally written in matrix form as given below:

$$Kq + C\dot{q} + M\ddot{q} = f(t) \quad \text{…..…….. (3)}$$

Where, M = the mass matrix,

C = the damping matrix,

K = the stiffness matrix of a structure,

q = the vector of nodal displacements

f = the vector of excitation nodal forces.

In the harmonic analysis, it is presumed that the excitation forces are varied in time harmonically with a given frequency (ω), i.e. $f = Fe^{i\omega t}$ …..…….. (4)

Where, F = complex amplitudes of excitation forces, and $i = \sqrt{-1}$.

As a result of such excitation a linear structure vibrate with the same frequency and displacements can be expressed in the form: $q = Qe^{iwt}$ …..…….. (5)

Where, Q = vector of complex amplitudes of displacements.

Substituting these expressions for displacements and forces in equation (3) gives us the equation of harmonic vibration in frequency domain:

$$[K + iwC - \omega^2 M]Q = F \quad \text{…..…….. (6)}$$

In the harmonic analysis the complex vector of nodal amplitudes is calculated and corresponding to it stresses and strains are determined (if required).

The frequency range ($f_{max} - f_{min}$) and number of intervals *n* determine the frequency interval $\Delta\Omega$.

$$\Delta\Omega = 2\pi \frac{f_{max} - f_{min}}{n} \quad \text{…….. (7)}$$

The simulation will solve *n* frequencies, starting from Ω+ΔΩ [24, 25].

1.3.5.3 Solution methods for harmonic response analysis

There are two solution methods are available in ANSYS 16.2, viz. Full method and Mode Superposition method. A brief description of these two methods are presented below.

a) Full method

The full method is one of the simplest solution methods for harmonic response analysis. In the full method equation (6) is solved directly. The full method uses the full system matrices in order to compute the harmonic response. The matrices may be symmetric or unsymmetric.

The benefits of the full method are as follows:

- Easy to use
- Uses full matrices, therefore no involvement of mass matrix approximation.
- The full method permits unsymmetric matrices.
- Can calculates entire displacements and stresses in a single pass.
- Allows all types of loads viz. imposed non-zero displacements, nodal forces, and element loads (pressures and temperatures).
- Allows efficient usage of solid-model loads.

The main disadvantage of the full method is that this method is more expensive as compared to the other methods [24, 25].

b) Mode superposition method

The Mode Superposition method is the default solution option and is available in ANSYS. Mode superposition method uses modal properties; therefore, the reduction procedure in the mode superposition method requires preliminary modal analysis. In the mode superposition method

reduction of the model is performed by expressing all degrees of freedoms (DOFs) through a superposition of natural mode shapes of a structure.

$$\underbrace{\{Q\}}_{N\times 1} = \sum_{j}^{n_m} \phi_j c_j = \Phi_j \qquad \text{…….. (8)}$$

The matrices for reduced equation of motion are calculated as follows:

$$K^r = \Phi^T K \Phi \; ; \quad M^r = \Phi^T M \Phi \; ; \; C^r = \Phi^T C \Phi \; ; \; F^r = \Phi^T F;$$

The mode superposition method sum ups factored mode shapes from a modal analysis in order to calculate the structure's response.

The major advantages of mode superposition method are given below:

- Faster and cheaper as compared to other solution methods for many problems
- Permits solutions to be clustered about the structure's natural frequencies. This results in a smoother, more accurate tracking of the response curve.
- Prestressing effects can be included.
- Allows modal damping (damping ratio as a function of frequency) [24, 25].

Chapter 2

Literature Review

2.1 Introduction to the literature review

In gas turbine engines, turbine blades are the most stressed elements, which play a very important role towards the safety and efficiency of a gas turbine engine. Owing to the significance of gas turbine blades, directionally solidified monocrystalline blades have been widely used in gas turbine engines because of their higher thermo-mechanical fatigue, thermal resistance, melt resistance capabilities and stress rupture [19, 26, 27, 28]. Previously, a huge number of studies has been carried out on the effect of anisotropic orientation on creep strength, elastic stress and fatigue lifetime [29, 30]. But, the effect of crystal orientations on dynamic characteristics like natural frequencies, mode shapes and forced responses of gas turbine bladed discs are lesser known. Therefore, there is a strong demand for in-depth literature review and analysis of effect crystal orientation on the dynamic characteristics of gas turbine bladed disc with an anisotropic material.

2.2 Overview of earlier research works

2.2.1 Anisotropic materials and their mathematical representation

Hu, X., Yang, X., Shi, D., Yu, H., and Ren, T., (2016), have performed a constitutive modelling of super alloy DZ125 (a directionally solidified nickel-based superalloy) subjected to thermal mechanical creep-fatigue loadings. In this literature, they have described a number of important mechanical and chemical properties of nickel-based DZ125 superalloy along with its chemical composition [2].

Dinçkal, Ç. (2012) has presented a study on a decomposition method based on orthonormal representations, and developed the decomposition method in order to examine the mechanical & elastic properties of an anisotropic material possessing any material symmetry and to govern anisotropy degree of the material [15].

2.2.2 Influence of material anisotropy on mechanical & elastic properties of turbine bladed disc with single-crystal blades

Savage, M.W.R., (2011), has accomplished a study on the effect of material anisotropy on the elastic stresses of a single crystal nickel-based turbine blade. He has evaluated material anisotropy effects elastic stresses of a single blade for 81 different orientations with 20 primary axis locations. The author concluded that, since the elastic constants change with direction, the orientation of the single crystal relative to the component has a direct influence on the elastic state of stress. Also, optimisation of the secondary angle at the blade root location may have an adversative outcome at some other blade locations, for example, the aerofoil and therefore the whole blade must be considered [18].

Hou, N.X., Gou, W.X., Wen, Z.X., and Yue, Z.F., (2008) and Arakere, N.K., and Swanson, G.R., (2002), have carried out a study on the effect of anisotropic orientation on creep strength, elastic stress and fatigue lifetime of monocrystalline anisotropic turbine blades. [29, 30].

2.2.3 Influence of material anisotropy on vibration characteristics of turbine bladed disc with single-crystal anisotropic blades

Kaneko, Y., Mori, K., and Ooyama, H. (2015) have accomplished a study on the resonant response and random response analysis of mistuned bladed disc with directionally solidified blade. They have used fundamental mistuning model and conventional modal analysis method in order to investigate the harmonic responses of the mistuned bladed disc. The results show that the maximum response of mistuned bladed disc with a directionally solidified blade is almost same as that of the conventional casting blades [31].

Wen, Z., Mao, H., Yue, Z. and Wang, B. (2013) have accomplished a research on the impact of anisotropic material orientations on vibration characteristics of nickel-based single crystal superalloy of the turbine blade. In this manuscript, the natural frequency of the blade has been calculated by the finite element method, and the results show that the deviation of the axial directions has an important effect on the lower frequency as well as on the higher frequency, whereas the randomness in crystallographic orientations has a great impact only on higher order frequency [19].

Fang, Y., and Li, Y., (2012) have studied on the dynamic responses of orthotropic nickel-based single crystal superalloy DD6 blade, considering the effect of temperature, rotor speed and orientation. Outcome of this study is that, the influence of rotor speed on natural frequencies of [001] orientation is greater than that of [111] and the natural frequencies of [111] orientation are higher than that of [001] i.e. the values of natural frequency are increased with the elevated rotor speed and decreased with the elevated temperature [32].

Kaneko, Y. (2011) has performed a study on the vibration characteristics of single crystal blade and directionally solidified blade. In this study, he has analysed the effect of anisotropy of elastic constants on the vibration characteristics of the monocrystalline and directionally solidified blades. Moreover, Monte Carlo simulation has been used to investigate the validity of the hypothesis of the transverse isotropy for directionally solidified models. Finally, sensitivity analysis method has been used to evaluate the frequency deviation of single crystal and directionally solidified blades [33].

Manetti, M., Giovannett, I., Pieroni, N., Horculescu et al.,(2009) have accomplished a study on the relation between lattice orientation and bucket vibration by using both experimental testing and finite element method [34].

Swanson, G.R., and Arakere, N.K., (2000), have carried out a study on the influence of crystal orientation on analysis of single-crystal turbine blade with nickel-based superalloys. In this article, they have explained about the blade material coordinate system relative to the casting coordinate system, and crystallographic orientations. He has evaluated material anisotropy effects on natural frequencies and mode shape of a single blade for 297 different orientations with 33 primary axis cases [20].

Habese, T. et al. (1994) and Kanko, Y. (2011) have carried out a study on the influence of material anisotropy on vibration characteristics of monocrystalline blades based on cantilever free vibration plates [35, 36].

2.2.4 Influence of material anisotropy on vibration characteristics of turbine bladed disc with composite blades

Kim, T., Hansen, M., A., and Branner, K., (2013) have carried out a study on the development of an anisotropic beam finite element for composite wind turbine blades in the multibody system. This manuscript explains a new anisotropic beam finite element for composite wind turbine blades and applied into the aeroelastic nonlinear multibody code, HAWC2; intended to be improved performance namely increased power capture and reduction of loads [37].

2.2.5 Various techniques and strategies for the dynamic analysis of tuned and mistuned bladed discs and their outcomes

Pohle1, L., Scheidt, L. P., and Wallaschek, J. (2015) have accomplished a study on harmonics mistuning of the bladed disc. In this article, the harmonic mistuning has been presented to evaluate the maximum amplitude for a given mistuning limit, where the separation of two orthogonal nodal diameters has been described in detail. Moreover, the excitation of more than one nodal diameter by only one engine order has been discussed [38].

Strnad, J., and Liska, J. (2015) have stated the significance of structural analysis of bladed discs of gas turbines. He has developed new diagnostic methods in order to evaluate the mode shape of bladed disc used for shrouded blades in steam turbines in terms of the wheel vibration and blade service time consumption as parts of the non-contact vibration monitoring system [39].

Nair, S., Nair, S., Chhabra, T., Verma, P., and Mittal, S., (2014) have performed a study on steady state structural analysis of high pressure gas turbine blade. Observed result of this study is that the root of the blade is subjected to the maximum stress and the blade section near the root has higher stress values compared to the tip of the blade. It is also found that titanium alloy exhibits the least amount of stress and undergoes very less deformation [1].

Vishwanatha, R.H., Zameer, S., and Haneef, M., (2014) have performed a study on finite element structural integrity analysis of first stage gas turbine rotor blade of Ni-Crome alloy assembly under thermo-mechanical loads. To determine structural safety and resonance frequency respectively,

coupled field analysis and model analysis has been carried out by considering rotational load and gas load. The results demonstrate that the developed stresses and deflections are within the allowable limit [40].

Babu1, J. S., Venkata, A.K.G., and Kumar, B.S.P., (2013) have carried out a study on dynamic response prediction of tuned and mistuned bladed disc of forged alloy steel. They found that the mistuned responses can exceed tuned response levels by about 200 percent. Moreover, the presence of localisation phenomenon has been observed in industrial turbomachinery rotor, which causes a significant increase in the amplitude of the forced response of the rotor [41].

Kaneko, Y., Ohta, M., Mori, K., and Ohyama, H., (2012) have carried out a study on resonant response reduction of mistuned bladed discs due asymmetric vane spacing by using an equivalent mass-spring model of the bladed disc and Monte Carlo method. The aftermath of this study is that for the mistuned bladed disc, the asymmetric vane spacing is effective to reduce the resonant response [42].

Rahimi, M., and Ziaei-Rad, S., (2009) have explained the fundamental technique of mistuning. Moreover, they have represented a method for exact evaluation of the harmonic forced response of mistuned bladed disc which is based on a connection between tuned and mistuned systems. A bladed disc with 56 blades having two degrees of freedom per blade has also been demonstrated to show the mistuning phenomena and the abilities of the suggested techniques. The results show that rearrangement is an effective way to reduce the worst-case harmonic forced response of bladed-disc system without any additional cost in the design of turbomachine. The aftermath of this study is that the rearrangement technique is more efficient as compared to intentional mistuning [8].

Nikolic, M., Petrov, E.P., and Ewins, D.J., (2008) have carried out a study on robust strategies for reduction of harmonic forced response of bisks based on the concept of large mistuning. In this paper they have introduced a robust technique for reduction of maximum harmonic forced response based on a concept of large mistuning, comprising both random and deterministic approaches. They have also demonstrated deterministic intentional mistuning method, which represents a considerable reduction in maximum forced response. The outcomes from this study illustrate various ways of

implementing the large mistuning concept into the design of gas turbine bladed discs in order to avoid largely forced response levels produced by random mistuning [43].

Yana, Y.J., Cuia, P.L., and Haob, H.N., (2008) have carried out a research on vibration mechanism of a mistuned bladed-disc; and concluded with some important findings regarding mistuned bladed discs that the natural frequency of a mistuned bladed-disc is denser and has a wider scattering; mode shape of the mistuned bladed-disc are of excessively large amplitudes in few blades; resonance range of the mistuned bladed-disc is much higher than the tuned bladed-disc; and random mistuned distribution with a small frequency variance should have a minor harmonic forced response and be easy to be realised [44].

Martel, C., and Corral, R., (2008) have performed a study on the asymptotic explanation of the maximum mistuning amplification of the harmonic forced response of bladed disc. They have used a perturbation methodology, the Asymptotic Mistuning Model for the amplification process, and to calculate the maximum mistuning amplification factor. Finally, the results of the asymptotic mistuning model have been validated numerically by using a simple mass-spring model [45].

Nikolic, M., Petrov, E. P., and Ewins, D.J., (2007) have determined the mutual impact of the influences of Coriolis forces and blade mistuning on dynamic characteristics of bladed discs; and established whether the Coriolis forces should be involved as a missing link in the analyses of mistuned blisks. It is found that the influences of Coriolis forces may have significant implications for estimation and interpretations of the harmonic forced response behaviour of mistuned bladed discs [46].

He,Z., and Epureanu, B., (2007) have carried out a study on effects of fluid-structural coupling on the dynamics of mistuned bladed discs. In this paper they have mentioned about various aeroelastic models that are used to investigate the forced response and free vibration problems of mistuned bladed disks, where most of these models used simplified structural models or aerodynamic models. In this research, a new reduced-order modelling approach has been established by using the tuned system modes in order to compute the unsteady aerodynamic forces directly. The aftermath of this study is that aerodynamic coupling has substantial effects on the vibration of bladed disks. Moreover, use of

the tuned system models to analyse the unsteady aerodynamic forces saves a substantial amount of computational time as that of both constraint modes and cantilever-blade normal modes [47].

Castanier, M.P., and Pierre, C., (2006) have introduced the status and emerging directions of modelling and analysis of mistuned bladed disc vibration. They have appraised reduced order modelling and analysis of the vibration of bladed discs of gas turbine engines and emphasised on better estimation and understanding of harmonic forced response of mistuned bladed discs in terms of assessing and mitigating the destructive impact of mistuning on blade vibration, stress increases, and attendant high cycle fatigue [11].

Rao J. S., (2006) has performed a research on mistuning of bladed disc assemblies to mitigate resonance. He has adopted modal distortion technique to diminish the mistuning effects and regulate resonant response in order to determine the worst case of mistuning and to determine the amplification factors [3].

Petrov, E.P., and Ewins, D.J., (2005) have accomplished a study on the method for analysis of nonlinear multi-harmonic vibrations of mistuned blisks with scatter of contact interface characteristics, and developed an effective technique for the analysis of nonlinear vibrations of mistuned bladed disk assemblies, which facilitates the use of large-scale finite element models for realistic bladed discs [48].

Choi, Y. S., Gottfried, D.A., and Fleeter, S., (2004) have developed a mathematical model in order to investigate the effects of aerodynamic damping on the maximum amplification factor of mistuned bladed discs. The relative impact of aerodynamic effects has been evaluated by a comparing an aerodynamic damping factor with the structural damping factor. Comparison of model results to data shows that including unsteady aerodynamic damping improves the prediction [5].

Petrov, E.P., and Ewins, D.J., (2003) have performed a research on the analysis of the worst mistuning patterns in bladed disk assemblies. They have developed a technique in order to calculate for practical mistuned bladed discs, the mistuning patterns that provide the highest response levels [49].

Petrov, E.P., and Ewins, D.J., (2003) have studied on analysis of the worst mistuning patterns in bladed disc assemblies. In this study, the problem of evaluating the worst mistuning patterns has been

formulated and resolved as an optimisation problem for large finite element models. Moreover, an effective method has been established to calculate the sensitivity coefficients for a maximum forced response regarding blade mistuning [7].

Petrov, E.P., Sanliturk, K.Y., and Ewins, D.J., (2002) have performed a research on a new technique for dynamic analysis of mistuned bladed discs based on the exact relationship between tuned and mistuned systems. The key benefits of the technique are its effectiveness and accurateness that permit the use of large finite element models of practical bladed disk assemblies in parametric studies of mistuning effects on vibration amplitudes [50].

Petrov, E., Sanliturk, K., Ewins, D., and Elliott, R. have introduced a method to analyse forced response of bladed discs which is based on the exact relationship between response level of the tuned and mistuned bladed discs. This literature also describes an exact relationship between the response amplitudes of the tuned and mistuned bladed discs and also explains how the tuned system could be used during the forced response analysis of a mistuned assembly [10].

Moyroud, F., and Fransson, T., (2002) have carried out a study on comparative analysis of two finite element reduction techniques applied to full assembly free vibration analyses of tuned and mistuned bladed discs. The first technique is based on a modal decomposition of a full assembly mistuned bladed disc and the second technique is based on a Craig and Bampton sub-structuring and reduction of the full assembly bladed disc. These two reduced-order models have been compared to three representative test rotors. [51].

James, B. M., (2001) has accomplished a study on reduced-order blade mistuning analysis methods developed for the robust design of engine rotors. In this study, they have made an important progress in the development of the component mode mistuning and static mode compensation approaches for reduced-order modelling of mistuned bladed discs. Static mode compensation methods has been developed for the modelling of large mistuning or geometric blade variations, moreover the author has investigated on modelling and forecasting the effects of mass mistuning; enhancements and major developments have been made in the turbo-reduce code for reduced-order modelling and analysis of

mistuned bladed discs and key observations were made on frequency veering analysis for finding critical operating situations [4].

Yang, M.T., and Griffin, J.H., (1999) have developed a reduced order model of mistuned bladed discs in which the modes of the mistuned system are represented in terms of a subset of nominal system modes [52].

Sinha, A., and Chen, S. (1989) have developed a higher order technique to compute the statistics of forced response of a mistuned bladed disc assembly. They have assumed the model stiffness of each blade to be a random variable with a Gaussian distribution. The validation of the analytical technique has been established by comparing the results with numerical simulations [6].

Kaza, Krishna R.V. and Kielb, R.E., (1984) have carried out a study on vibration and flutter of mistuned bladed-disc assemblies. They have developed an analytical model and an associated computer program in order to investigate the special influence of disc flexibility on vibration and flutter characteristics of both tuned and mistuned bladed-disc assemblies. One of the relevant and important conclusion they have made is that a moderate amount of blade frequency mistuning has strong potential to rise the flutter speed, even in the presence of the mechanical coupling between blades that is introduced by disc flexibility [9].

2.3 Conclusions to the literature review

In this chapter a number of articles have been reviewed which are relevant to the current research topic. More specifically, literatures have been reviewed on the effects of crystal orientations on mechanical and dynamic properties of a turbine bladed disc with an anisotropic material blade (including composites and directionally solidified single crystal blades). Also, literatures have been found on the mathematical representation of anisotropic material and about mechanical, elastic and chemical properties of anisotropic materials. From the entire literature review, it is obvious that- although a wide range of research has been performed on various aspects of mistuned and tuned bladed disc of gas turbines, but very few literatures have been found which investigates the effect on anisotropic material orientations on the dynamic properties of a bladed disc with monocrystalline

anisotropic blades. Likewise, no literature has been found in the analysis of tuned and mistuned bladed disc with DZ 125 nickel based superalloy. Therefore, there is a strong need for the analysis of the effects of crystal orientation on the dynamic characteristics of gas turbine bladed disc with a single crystal anisotropic blade material. Based on the above literature review, it is evident that the findings of the current study would be quite important for further research in the related field.

Chapter 3

Methodology for the Dynamic Analysis

This chapter describes the key steps that were involved in the creation of geometry for different dynamic analyses in order to achieve the proposed objectives. This chapter also represents a decent description of the research methodology that was used during this study. It includes the selection of material for blade & disc, meshing, and the techniques and strategies used during modal analysis and forced response analysis in order to evaluate the effects of anisotropy on modal properties of a single blade and a tuned bladed disc; moreover, to appraise the effects of material anisotropy on forced responses of mistuned bladed disc.

3.1 Creation of the models

The design of proposed models of the bladed disc has been carried out by modifying the original model of a sector of a bladed disc of gas turbine. The original model of the sector of the bladed disc is shown in Figure 5.

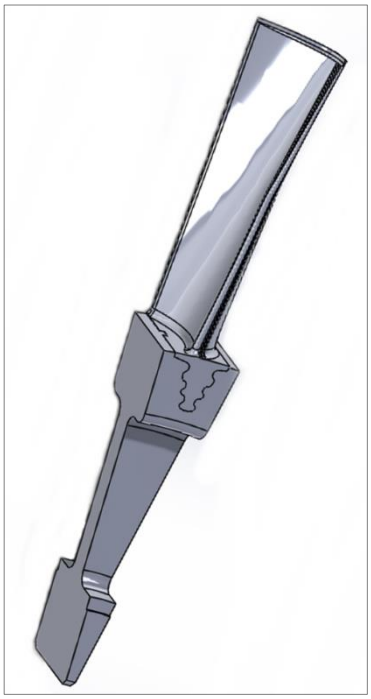

Figure 5: Original design of the bladed disc sector model

3.1.1 Creation of the single blade FE (finite element) model

In order to analyse the material anisotropy effects on natural frequencies and mode shape of a single blade, a single blade model was created in the SolidWorks from the original model.

In order to reduce the number of finite elements in the blade, the original model of the blade was modified in a number of stages. Initially, the model was simplified in SolidWorks. After a series of operations in SolidWorks and in ANSYS SpaceClaim, a new model was generated which is shown in Figure 6.

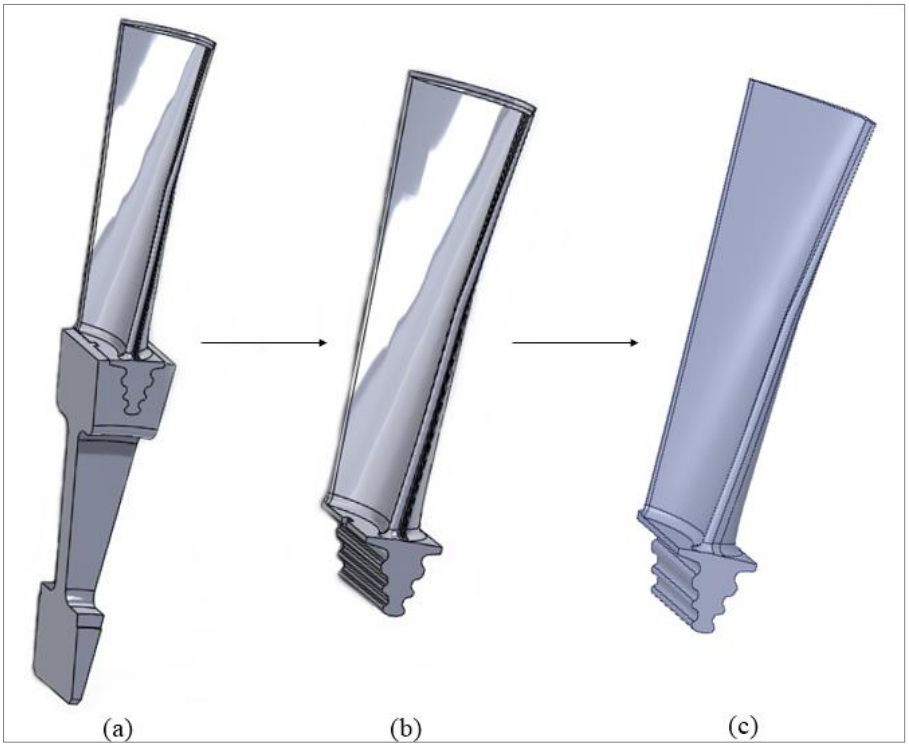

Figure 6: Different stages of the design of a single blade model

In the Figure 6, the figure (a) represents the original design of the sector model, figure (b) shows a single blade extracted from the original sector model in SolidWorks, figure (c) represents the final simplified design of the single blade model after a series of operations in SolidWorks and in ANSYS SpaceClaim. Here, the original blade was simplified by cutting the complex design at the top edge of the original blade that was created from the original sector model, afterwards small faces were merged in ANSYS SpaceClaim to reduce the number of finite elements in the blade model.

Then the single blade model was meshed in ANSYS Workbench, as shown in Figure 7. Also, specification of the finite element mesh is presented in Table 1

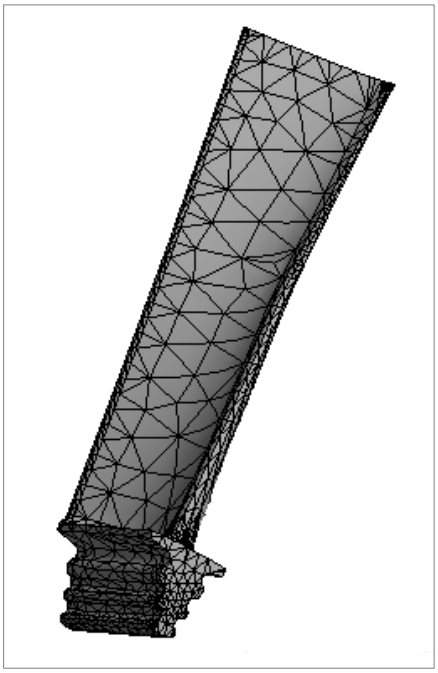

Figure 7: Single blade model with finite element mesh

Table 1: Specifications of the finite element mesh of the single blade model

Particulars	Specifications
Total number of elements	3486
Total number of nodes	6938
Element type	Quadratic tetrahedron

3.1.2 Creation of the sector FE model

In order to analyse the effects of material anisotropy orientation on natural frequencies and mode shape of a tuned bladed disc, a sector model was created by modifying the original sector model in SolidWorks. The main intention of this modification is to reduce the number of finite elements.

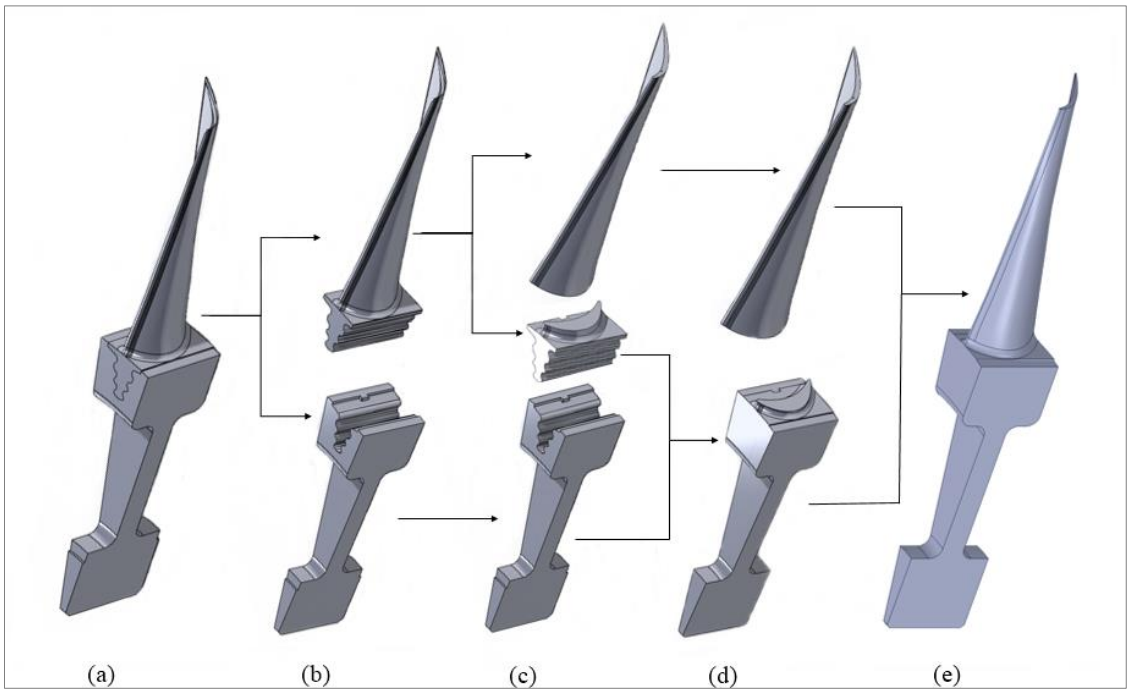

Figure 8: Different stages of the design and modification process of the bladed disc sector model

There were so many uneven and small surfaces in the SolidWorks modified model, which leads to increase in the number to finite elements. Therefore, the model was simplified in ANSYS SpaceClaim by merging small surfaces. The final design of the bladed disc sector was obtained after a series of operations in SolidWorks and ANSYS SpaceClaim, which can be seen in Figure 8. Where, the figure (a) shows the original sector model, figure (b) shows the splitting of sector into two parts (blade and disc sector), in figure (c) the blade was cut into two parts, figure (d) shows the bottom portion of the blade was assembled with disc sector, and finally the figure (e) shows the final design of the sector model after a series of operations in SolidWorks and SpaceClaim.

Subsequently, the sector model of the bladed disc was meshed in ANSYS Workbench, as presented in Figure 9. Also, specification of the finite element mesh is presented in Table 2

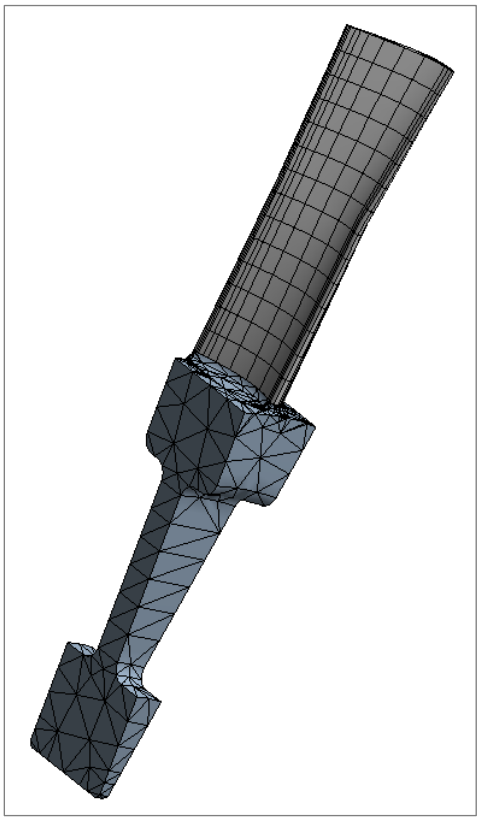

Figure 9: Sector model of a bladed disc with finite element mesh

Table 2: Specifications of the finite element mesh for the sector model

Particulars	Specifications
Total number of elements	2012
Total number of nodes	5128
Element type (Disc)	Quadratic tetrahedron
Element type (Blade)	Quadratic hexahedron

3.1.3 Creation of the FE models for whole bladed disc: tuned and mistuned models

In order to analyse the harmonic forced response of a bladed discs with mistuning due to material anisotropy, a whole bladed disc model was created from the sector model (as presented in Figure 8 and Figure 9) in ANSYS Workbench by using Pattern tool. The final design of the whole bladed disc model comprises of 30 numbers of sectors as shown in Figure 10.

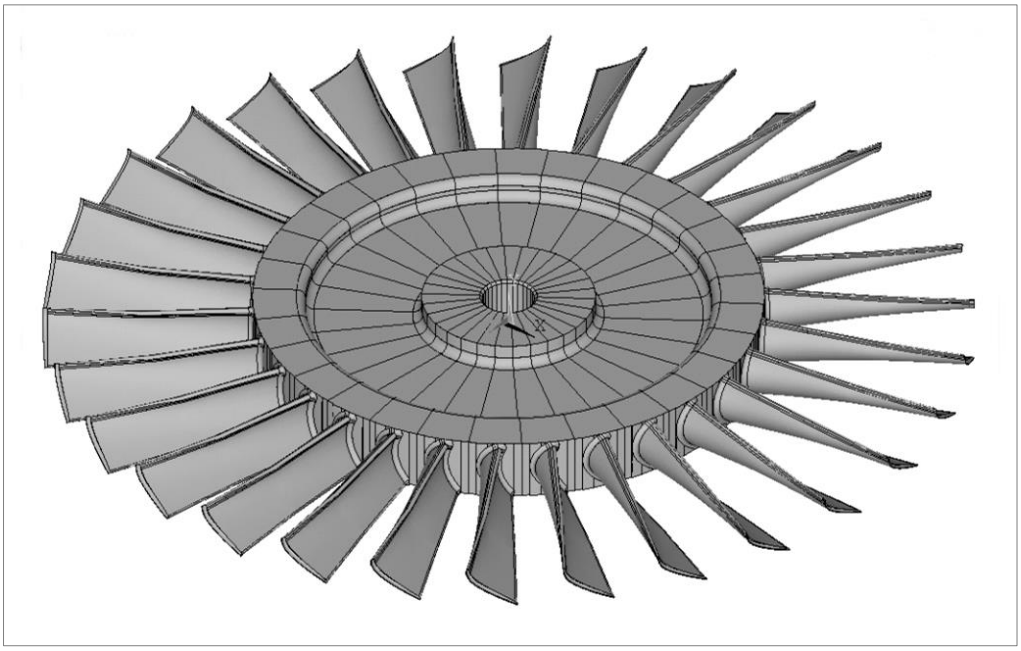

Figure 10: Whole bladed disc model

Afterwards, the whole bladed disc model was meshed in ANSYS Workbench, as shown in Figure 11. Also, the specification of the finite element mesh was presented in Table 3.

Table 3: Specifications of the finite element mesh of the bladed disc model

Particulars	Specifications
Total number of elements	57750
Total number of nodes	114810
Element type (Disc)	Quadratic tetrahedron
Element type (Blade)	Quadratic hexahedron

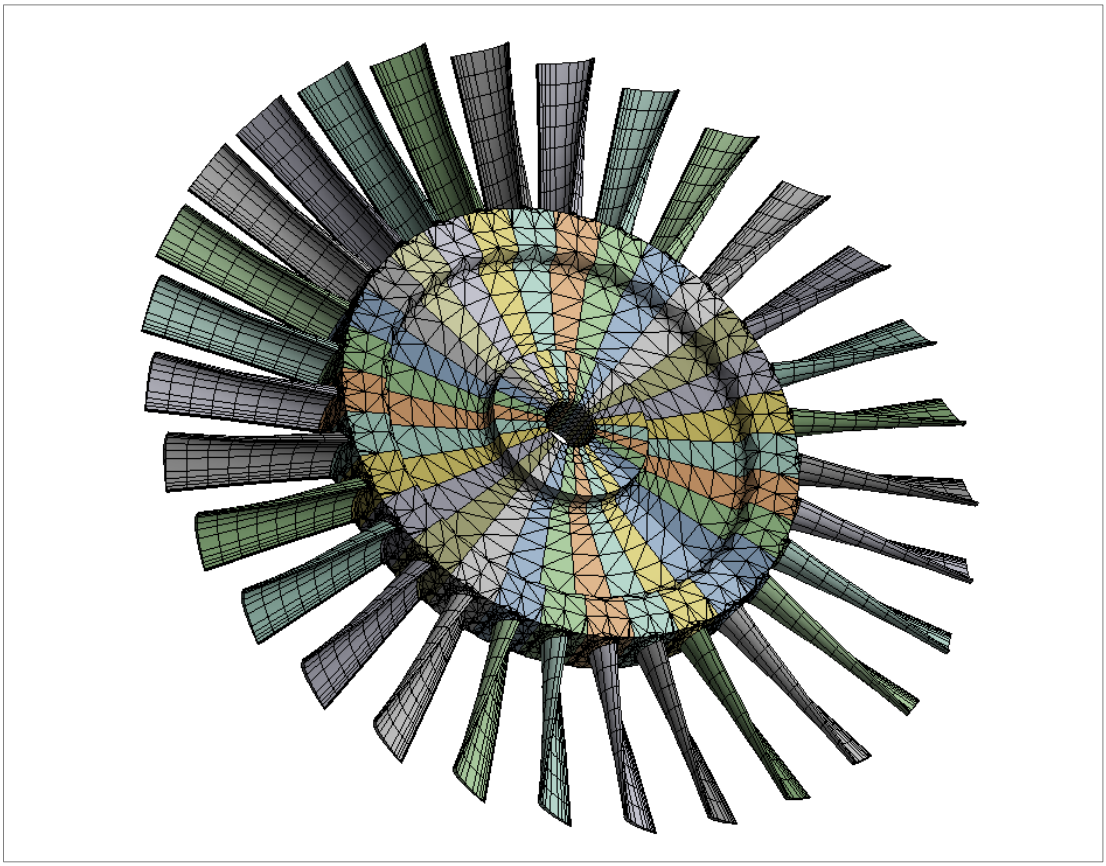

Figure 11: Bladed disc with finite element mesh

3.2 Finite elements

This section describes a brief overview of the finite elements that were used during the mesh generation of the above-mentioned geometries. Types of finite elements used are Quadratic Tetrahedron and Quadratic Hexahedron.

3.2.1 Quadratic tetrahedron

As presented in Figure 12, a Quadratic Tetrahedron is a higher-order 3-D, 10-node element. This element has three degrees of freedom per node, translations in the nodal x, y, and z directions. The quadratic tetrahedron supports creep, plasticity, hyperelasticity, stress stiffening, large deflection, and large strain capabilities. Also, it has the capability of mixed formulation for simulating deformations of fully incompressible hyperelastic materials and nearly incompressible elastoplastic materials. This type of element is particularly attractive because of the existence of fully automatic tetrahedral

meshers. This element possesses a quadratic displacement behaviour and suitable to modelling irregular meshes, especially for the geometries produced from various CAD/CAM systems [53, 54].

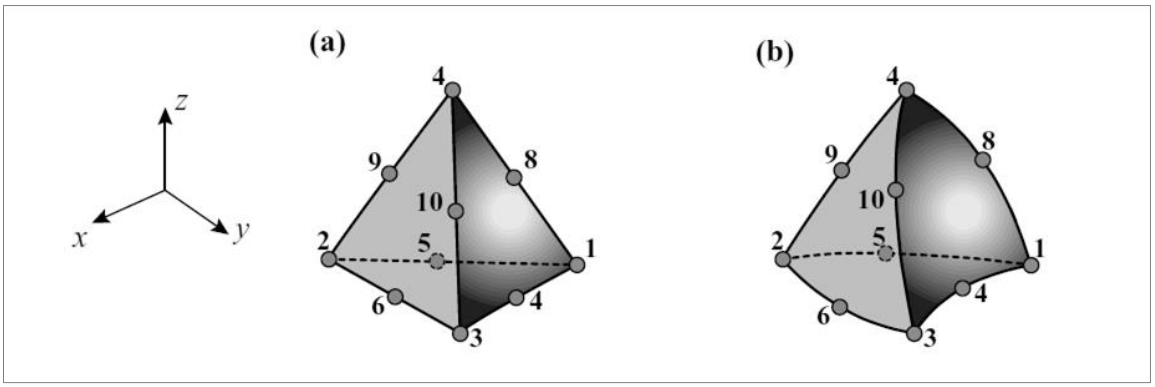

Figure 12: The quadratic (10 nodes) tetrahedron. (a) An element with planar faces and side nodes located at side midpoints; (b) An element with curved faces and sides [53].

3.2.2 Quadratic hexahedron

The Quadratic Hexahedron is a higher order 20-node solid element possessing three degrees of freedom per node, translations in the nodal x, y, and z directions. This element supports plasticity, hyperelasticity, creep, stress stiffening, large deflection, and large strain capabilities. This element is an excellent element for linear elastic calculations. Also, it has the capability of mixed formulation for simulating deformations of nearly incompressible elastoplastic materials, and fully incompressible hyperelastic materials. A quadratic hexahedron is shown in Figure 13 [55, 56].

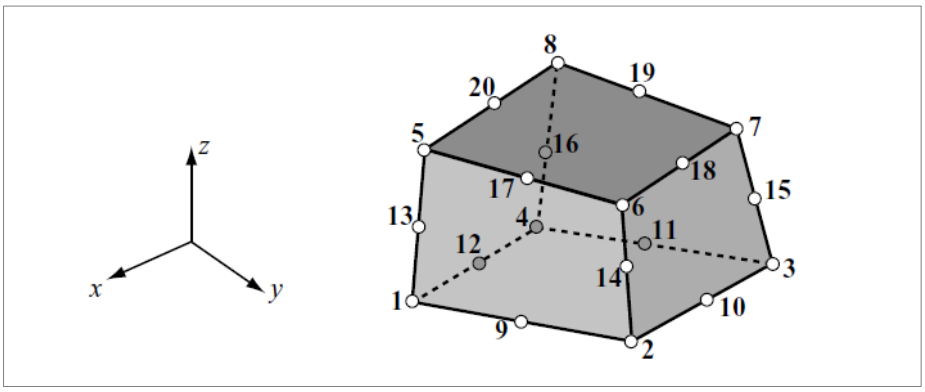

Figure 13: The quadratic (twenty-node) hexahedron element [55]

3.3 Material Selection

Gas turbine materials play a significant role in building gas turbine engines with higher power ratings and efficiency levels. These materials should possess a number of qualities including the - capability of the materials to withstand elevated temperature service, very high strength to weight ratio, high level of mechanical properties and excellent resistance to oxidation or hot corrosion etc.

A wide range of high-performance materials viz. special steels, titanium and nickel-based alloys and superalloys, ceramics, composites and intermetallics are generally used for the construction of gas turbines [1- 4]. In this study, Nickel based superalloy DZ125 is used as a monocrystalline blade material, on the other hand nickel-iron-chromium alloy 706 is used as a disc material.

3.3.1 Blade material

DZ125 is a directionally solidified Nickel based superalloy, which is used for turbine blades and vanes. The chemical compositions of the superally DZ125 are presented in Table 4.

Table 4: Chemical composition of DZ125 superalloy

C	**Co**	**Cr**	**Mo**	**Ti**	**W**	**Al**	**Ta**
0.07–0.12	9.5–10.5	8.4–9.4	1.5–2.5	0.7–1.2	6.5–7.5	4.8–5.4	3.5–4.1
B	**Ni**	**Hf**	**Si**	**Mn**	**Zr**	**Fe**	**S**
0.01–0.02	Bal.	1.2–1.8	≤0.15	≤0.15	≤0.08	≤0.30	≤0.01
P	**Sn**	**As**	**Sb**	**Bi**	**Sb**	**Ag**	
≤0.01	≤0.001	≤0.001	≤0.0005	≤0.00005	≤0.001	≤0.0005	

Mechanical properties viz. Young's modulus (E), Shear modulus (G) and Density (ρ) of superalloy DZ125 at 700^{o} C is given below:

$E_x = E_y = 145.5$ GPa, $E_z = 104.5$ GPa

$G_{xy} = 56.5$ GPa, $G_{yz} = G_{xz} = 92.5$ GPa

Density (ρ) = 8450 kg/m^3

Now, Poisson's ratios (ν) can be calculated by using the following co-relations:

$$\nu_{xy} = \frac{E_y}{2G_{xy}} - 1 = \frac{145.5}{2\times 56.5} - 1 = 0.2876 \quad \text{…….. (9)}$$

$$\nu_{yz} = \frac{E_z}{2G_{yz}} - 1 = \frac{104.5}{2\times92.5} - 1 = -0.4351 \quad \text{…….. (10)}$$

$$\nu_{xz} = \frac{E_z}{2G_{xz}} - 1 = \frac{104.5}{2\times92.5} - 1 = -0.4351 \quad \text{…….. (11)}$$

3.3.2 Disc material

The material selected for the disc material is the nickel-iron-chromium alloy 706. The chemical compositions of the 706 alloy are listed in Table 5 [57].

Table 5: Chemical composition of alloy 706

Ni (plus Co)	**Ch**	**Fe**	**Nb (plus Ta)**	**Ti**	**Mn**	**C**
39.0-44.0	14.5-17.5	Balanced	2.5-3.3	1.5-2.0	≤0.15	0.06 max.
Cu	**Mg**	**Si**	**S**	**P**	**B**	**Co**
0.30 max.	0.35 max.	0.35 max.	0.015 max.	0.020 max.	0.006 max.	1.00 max

The Mechanical properties of alloy 706 at 700° C is given below.

E = 166 GPa, G =59 GPa, ν = 0.415, ρ = 8050 kg/m^3

3.4 Analysis of the effects of material anisotropy on modal properties of a single blade model

In order to evaluate the material anisotropy effects on natural frequencies and mode shape of a single blade, modal analysis of the single blade model was carried out for different anisotropic material orientations. The appearance of a single blade with Euler angles (Eulerian angles as described in the section 1.3.3 of chapter 1, Figure 2 and Figure 3) is shown in Figure 14. Modal analysis of the single blade was carried out for 225 different material orientations, having 10 modes for each orientation. Different anisotropic orientations of the monocrystalline blade are presented in Table 6 according to the Figure 15. The Figure 15 and Table 6 shows:

- 25 orientations (cases) of (φ and θ) with 9 (Ψ) orientations about each of these.
- 12 cases with (φ and θ) combined to 7.5°, 12 with (φ and θ) combined to 15°, 1 case with (φ and θ) combined to 0°.

- (Ψ) varied from 0° to 80° in 10° increments about the local material axis. (due to symmetry, 90° is the same as 0°).
- Total of 225 orientations (cases).

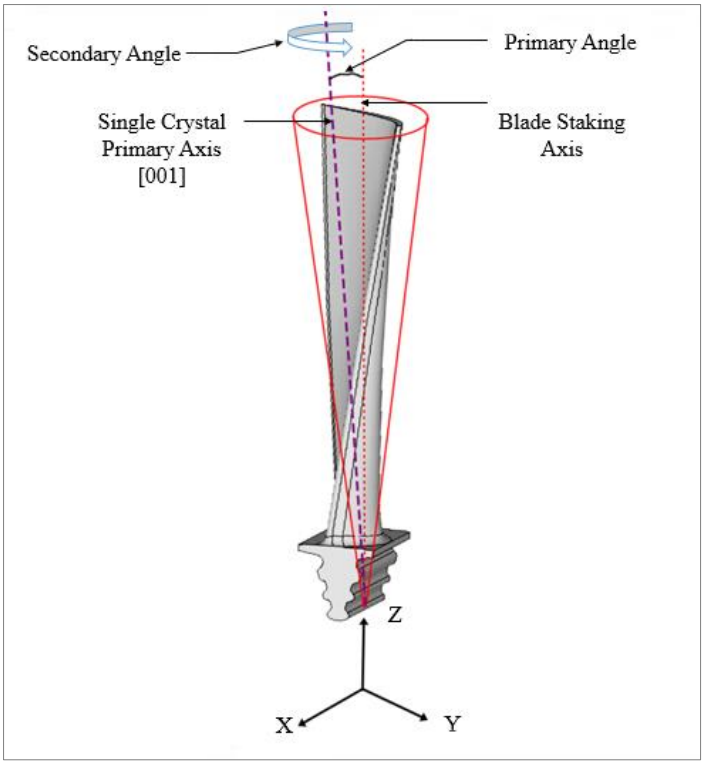

Figure 14: A single crystal turbine blade showing primary and secondary angles

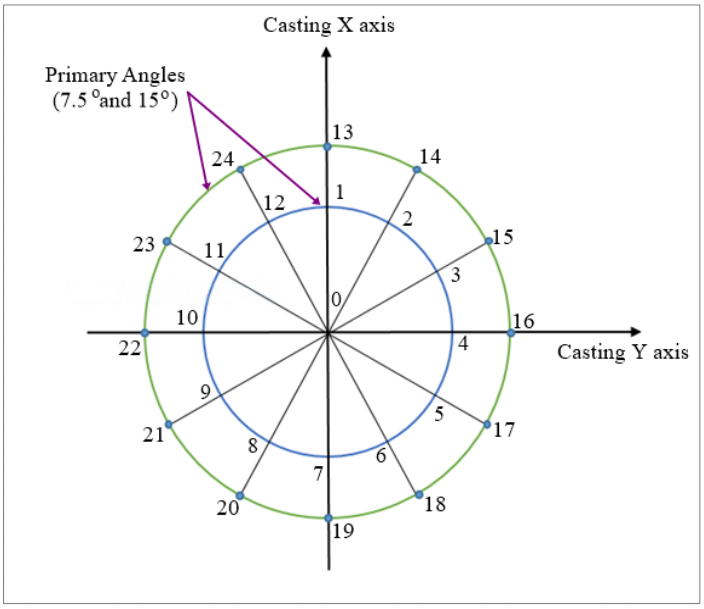

Figure 15: Plan view of the turbine blade demonstrating the locations of primary axis at two primary angles

Table 6: Simulated single-crystal material orientations for the single blade model

Case No.	φ (degree)	θ (degree)	Ψ (degree)
0	0	0	0, 10, 20, 30, 40, 50, 60, 70, 80
1	7.5	0	0, 10, 20, 30, 40, 50, 60, 70, 80
2	6.49	3.75	0, 10, 20, 30, 40, 50, 60, 70, 80
3	3.75	6.49	0, 10, 20, 30, 40, 50, 60, 70, 80
4	0	7.5	0, 10, 20, 30, 40, 50, 60, 70, 80
5	-3.75	6.49	0, 10, 20, 30, 40, 50, 60, 70, 80
6	-6.49	3.75	0, 10, 20, 30, 40, 50, 60, 70, 80
7	-7.5	0	0, 10, 20, 30, 40, 50, 60, 70, 80
8	-6.49	-3.75	0, 10, 20, 30, 40, 50, 60, 70, 80
9	-3.75	-6.49	0, 10, 20, 30, 40, 50, 60, 70, 80
10	0	-7.5	0, 10, 20, 30, 40, 50, 60, 70, 80
11	3.75	-6.49	0, 10, 20, 30, 40, 50, 60, 70, 80
12	6.49	-3.75	0, 10, 20, 30, 40, 50, 60, 70, 80
13	15	0	0, 10, 20, 30, 40, 50, 60, 70, 80
14	12.99	7.5	0, 10, 20, 30, 40, 50, 60, 70, 80
15	7.5	12.99	0, 10, 20, 30, 40, 50, 60, 70, 80
16	0	15	0, 10, 20, 30, 40, 50, 60, 70, 80
17	-7.5	12.99	0, 10, 20, 30, 40, 50, 60, 70, 80
18	-12.99	7.5	0, 10, 20, 30, 40, 50, 60, 70, 80
19	-15	0	0, 10, 20, 30, 40, 50, 60, 70, 80
20	-12.99	-7.5	0, 10, 20, 30, 40, 50, 60, 70, 80
21	-7.5	-12.99	0, 10, 20, 30, 40, 50, 60, 70, 80
22	0	-15	0, 10, 20, 30, 40, 50, 60, 70, 80
23	7.5	-12.99	0, 10, 20, 30, 40, 50, 60, 70, 80
24	12.99	-7.5	0, 10, 20, 30, 40, 50, 60, 70, 80

In order to define these anisotropic angles for the monocrystalline turbine blade material (DZ125) during the modal analysis of the single blade FE model, an APDL command was used as given below:

```
local,13,0,0,0,0,arg1,arg2,arg3,0,0     ! Create a new coordinate system with angular Z orientation = Arg1
esel,s,mat,,matid                       ! Select the elements for this Body
emodif,all,esys,13                      ! Change the element coordinate systems to 13
allsel                                  ! Select all elements
```

During modal analysis, fixed supports were introduced comprises of 15 surfaces at the bottom of the blade as shown in Figure 16, and finally 10 natural frequencies and mode shapes were evaluated.

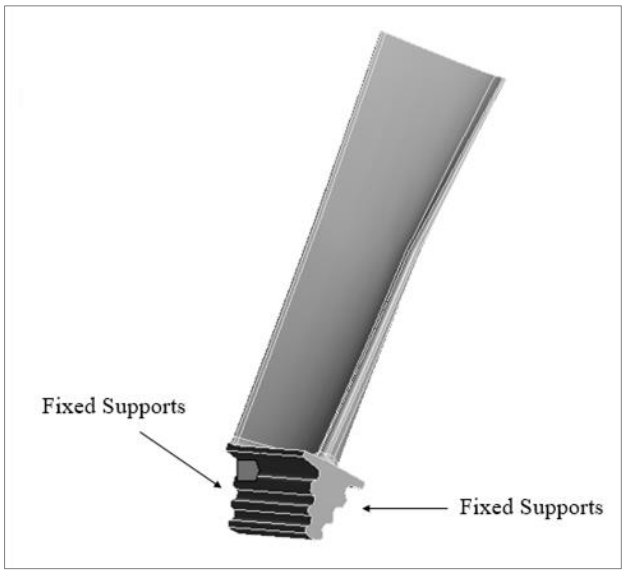

Figure 16: The blade model showing fixed supports

The solutions of these simulations with different anisotropic angles were studied to examine the influence of primary and secondary angle variations on the natural frequencies and mode shapes of the turbine blade. The results of this study are presented and discussed in section 4.1 of the chapter 4.

3.5 Analysis of the effects of material anisotropy on modal properties of a tuned bladed disc

Modal analysis of a tuned bladed disc was carried out in order to evaluate the effects of anisotropic material orientations on natural frequencies and mode shape of a tuned bladed disc. Modal analysis of the tuned bladed disc was performed using a cyclic symmetry model; the key advantage of using cyclic symmetry is to save CPU/elapsed time and computer resources [47].

During the analysis, a fixed support was introduced at the bottom of the sector as shown in Figure 17, and 10 mode shapes were calculated with harmonic index ranging from 0 to 15. An APDL command was used to define the anisotropic angles as mentioned earlier in section 3.4 of this chapter. Then, Parameter Set was used to create Design of Experiments (Design type: Face-Centred, Template type: Enhanced). The maximum and minimum value of primary angles that was defined during the generation of the design of experiments are given in Table 7. Subsequently, ANSYS automatically created 29 design points as presented in Table 8.

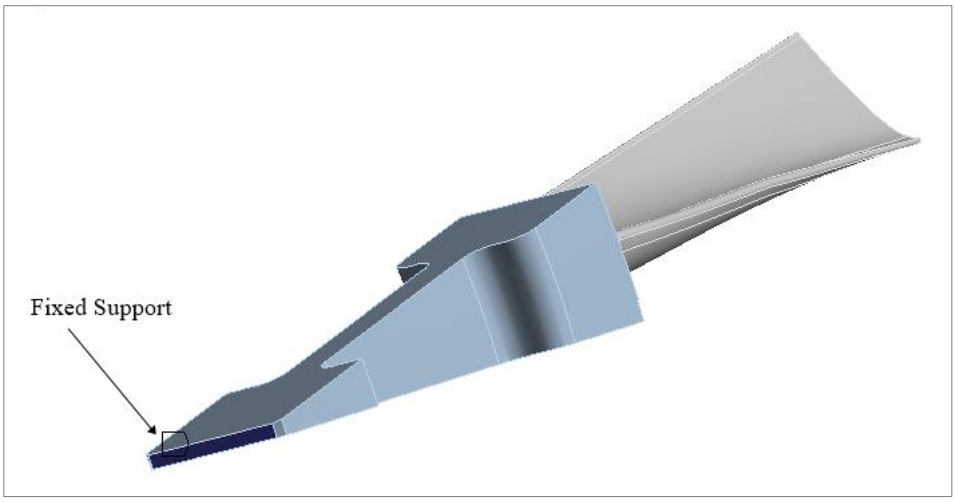

Figure 17: Sector model showing fixed support

A design point is a location within the response space, which is a result of a specific combination of input parameters. Automatic design points are generated based on the number of input parameters in the system, output parameter can be calculated for the automatically generated design points by using a regression analysis technique [58, 59].

The results of these simulations were analysed to investigate the effects of variation of Eulerian angles on the natural frequencies and mode shapes of a tuned bladed disc. The results of this study are presented and discussed in section 4.2 of chapter 4.

Table 7: Anisotropic angle ranges for the cyclically symmetric sector model (tuned bladed disc)

Angles	Lower Bound (degree)	Upper Bound (degree)
φ (primary angle)	-15	15
θ (primary angle)	-15	15
Ψ (secondary angle)	0	80

Table 8: Design points for anisotropic material orientations for modal analysis of the tuned bladed disc (cyclically symmetric sector model)

Design Points	φ (degree)	θ (degree)	Ψ (degree)
1	-15	40	0
2	-15	0	-15
3	-15	80	-15
4	-15	0	15
5	-15	80	15
6	-7.5	40	0
7	-7.5	20	-7.5
8	-7.5	60	-7.5
9	-7.5	20	7.5
10	-7.5	60	7.5
11	0	40	0
12	0	0	0
13	0	20	0
14	0	80	0
15	0	60	0
16	0	40	-15
17	0	40	-7.5
18	0	40	15
19	0	40	7.5
20	7.5	40	0
21	7.5	20	-7.5
22	7.5	60	-7.5
23	7.5	20	7.5
24	7.5	60	7.5
25	15	40	0
26	15	0	-15
27	15	80	-15
28	15	0	15
29	15	80	15

3.6 Analysis of the effects of material anisotropy on modal characteristics and forced response of a mistuned bladed disc

Forced response harmonic analysis of a mistuned bladed disc was carried out in order to evaluate the effects of anisotropic material orientations on the modal characteristic and forced responses of mistuned bladed disc.

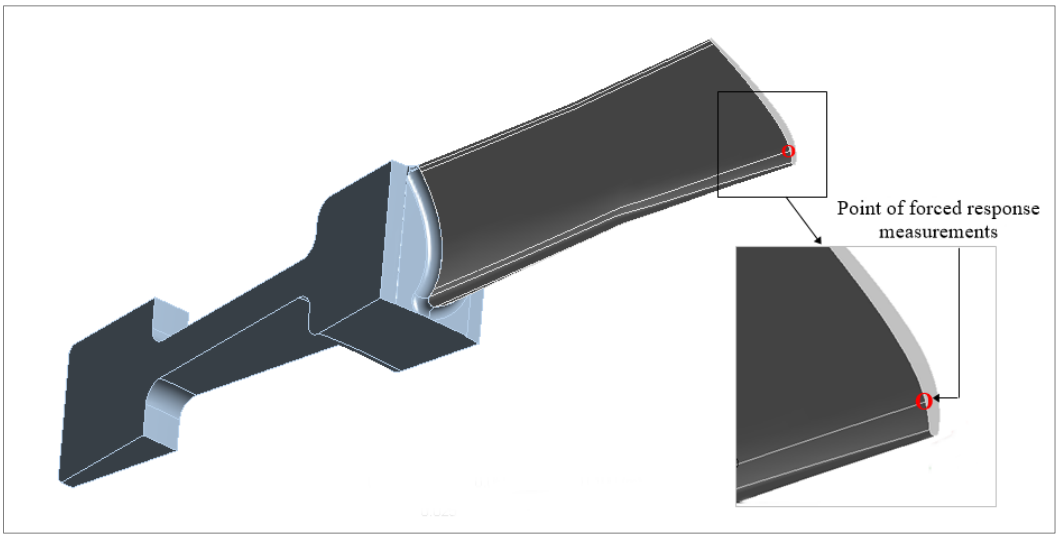

Figure 18: A sector of the bladed disc showing the location of forced response measurements

During harmonic analysis, fixed supports were introduced at the bottom edge of the disc. Forced response levels were calculated for 150 modes (frequency range 0 Hz to 2000 Hz) under second and fourth engine-order excitations (2EO and 4EO) using the homogeneous distribution of loads (1 Pa) along the blade. Harmonic forced responses for all 30 blades of the whole bladed disc were calculated at same locations (in the blade tip) as shown in Figure 18. The key specifications of the analysis setting are presented in Table 9.

Table 9: Specifications of the harmonic analysis

Particulars	Specifications
Solution method	Mode superposition
Maximum modes to find	150
Load type	Pressure (1 Pa)
Frequency spacing	Linear
Frequency range	0 Hz to 2000 Hz
Constant damping ratio	0.01
Cluster number	20

The interblade phase angles for each blade corresponding to the respective engine order excitations were calculated using the following formula:

Interblade phase angles, $\theta = \frac{2\pi k}{N}(j-1)$ …….. (12)

Where, N = Total number of blades in the bladed disc = 30

k = Engine order = 1 ... ... $\left(\frac{N}{2}\right)$, i.e. 1 to 15

j = Blade number = 1 ... ... N, i.e. 1 to 30

Moreover, a series of simulations were carried out using four mistuning patterns as presented in Table 10. Also, analyses were carried out for tuned bladed disc with anisotropic orientations ($\varphi = 0$, $\theta = 0$, $\Psi = 0$) in order to compare the solutions of tuned bladed disc with the results of mistuned bladed disc with four different mistuning patterns.

Table 10: Mistuning patterns for mistuned bladed disc analysis

Blade Number	**Mistuning Patterns (φ, θ, Ψ) in degrees**			
	1	**2**	**3**	**4**
1	(0, 0, 0)	(7.5, 0, 0)	(7.5, 0, 10)	(7.5, 0, 0)
2	(0, 15, 0)	(0, 0, 0)	(0, 0, 20)	(0, 0, 0)
3	(0, -15, 0)	(0, 15, 0)	(0, 15, 30)	(0, 15, 0)
4	(15, 0, 0)	(15, 0, 0)	(15, 0, 40)	(15, 0, 0)
5	(-15, 0, 0)	(15, 0, 0)	(15, 0, 50)	(15, 0, 0)
6	(7.5, 0, 0)	(7.5, 0, 0)	(7.5, 0, 60)	(7.5, 0, 0)
7	(-7.5, 0, 0)	(-7.5, 0, 0)	(-7.5, 0, 70)	(-7.5, 0, 0)
8	(0, 7.5, 0)	(0, -7.5, 0)	(0, -7.5, 80)	(0, -7.5, 0)
9	(0, -7.5, 0)	(0, 7.5, 0)	(0, 7.5, 0)	(0, 7.5, 0)
10	(3.75, 6.49, 0)	(3.75, 6.49, 40)	(3.75, 6.49, 40)	(3.75, 6.49, 0)
11	(3.75, -6.49, 0)	(3.75, -6.49, 10)	(3.75, -6.49, 10)	(3.75, -6.49, 0)
12	(-3.75, 6.49, 0)	(-3.75, 6.49, 20)	(-3.75, 6.49, 20)	(-3.75, 6.49, 0)
13	(-3.75, -6.49, 0)	(-3.75, -6.49, 30)	(-3.75, -6.49, 30)	(-3.75, -6.49, 0)
14	(7.5, 12.99, 0)	(7.5, 12.99, 50)	(7.5, 12.99, 50)	(7.5, 12.99, 0)
15	(-7.5, 12.99, 0)	(-7.5, 12.99, 60)	(-7.5, 12.99, 60)	(-7.5, 12.99, 0)
16	(7.5, -12.99, 0)	(7.5, -12.99, 70)	(7.5, -12.99, 70)	(7.5, -12.99, 0)
17	(0, 0, 0)	(0, 0, 80)	(0, 0, 80)	(0, 0, 0)
18	(0, 0, 70)	(0, 15, 70)	(0, 15, 70)	(0, 15, 0)
19	(-15, 0, 70)	(-15, 0, 70)	(-15, 0, 0)	(-15, 0, 0)
20	(0, -15, 40)	(0, -15, 40)	(0, -15, 0)	(0, -15, 0)
21	(-10, 0, 30)	(-10, 0, 10)	(-10, 12.99, 0)	(-10, 12.99, 0)
22	(0, -10, 30)	(0, 10, 30)	(0, 10, 30)	(0, 10, 0)
23	(-7.5, 0, 20)	(-7.5, 0, 20)	(-7.5, 10, 20)	(-7.5, 10, 0)
24	(0, -7.5, 20)	(0, 7.5, 20)	(0, 7.5, 20)	(0, 7.5, 0)
25	(7.5, 0, 10)	(7.5, 0, 0)	(0, 0, 20)	(0, 0, 0)
26	(0, 7.5, 0)	(0, -7.5, 0)	(0, 15, 70)	(0, 15, 0)
27	(15, 0, 60)	(15, 0, 60)	(15, 0, 0)	(15, 0, 0)
28	(0, -15, 50)	(0, 15, 50)	(10, 15, 0)	(15, 0, 0)
29	(0, 0, 0)	(0, -7.5, 40)	(0, 7.5, 0)	(7.5, 0, 0)
30	(0, 15, 0)	(0, -15, 0)	(30, -7.5, 0)	(-7.5, 0, 0)

The results of the above simulations were analysed to explore the effects of variation of anisotropic angles on the modal properties and harmonic forced response of a mistuned bladed disc. The results of this study are presented and discussed in section 4.3 of chapter 4.

Chapter 4

Results and Discussions

4.1 Effects of material anisotropy on modal properties of the single blade model

As mentioned in section 3.4 of chapter 3, modal analysis of a single blade was carried out for different anisotropic orientations of DZ125 alloy in order to evaluate the effects of anisotropic orientations on modal properties of a single crystal gas turbine blade. The results of the modal analysis with Euler angles ($\varphi = 0°$, $\theta = 0°$, $\psi = 0°$) is tabulated in Table 11, also different mode shapes corresponding to their natural frequencies are plotted in Figure 19.

Table 11: Natural frequencies and mode shapes of the single crystal blade with Eulerian angles ($\varphi = 0$, $\theta = 0$, $\psi = 0$)

Mode Shapes	Natural Frequencies (Hz)
1	319.57
2	762.98
3	1130.20
4	1385.30
5	2029.30
6	2652.60
7	3213.70
8	3851.10
9	4193.10
10	4420.00

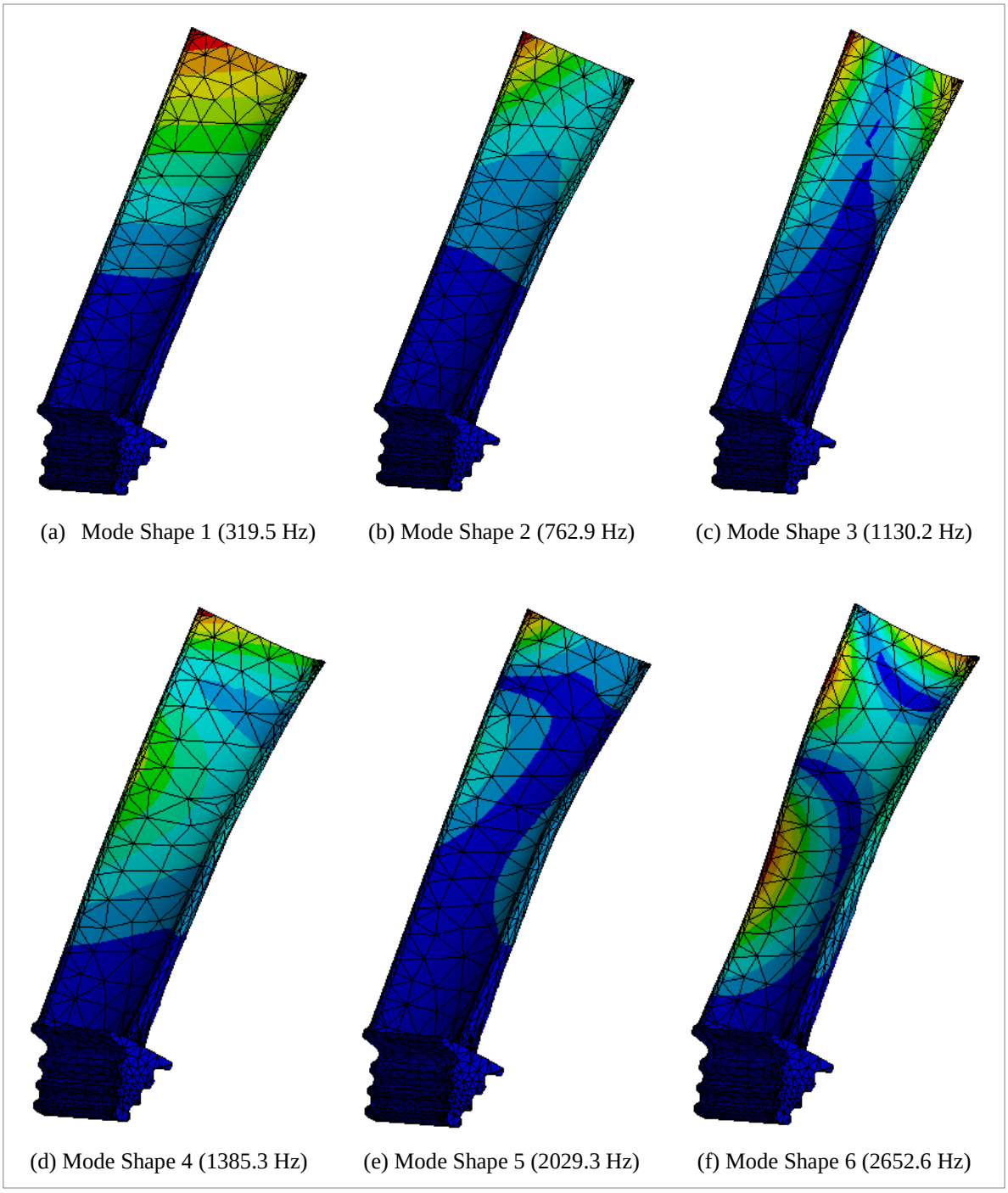

(a) Mode Shape 1 (319.5 Hz) (b) Mode Shape 2 (762.9 Hz) (c) Mode Shape 3 (1130.2 Hz)

(d) Mode Shape 4 (1385.3 Hz) (e) Mode Shape 5 (2029.3 Hz) (f) Mode Shape 6 (2652.6 Hz)

Figure 19: Different mode shapes of the DZ125 single crystal blade with their corresponding natural frequencies

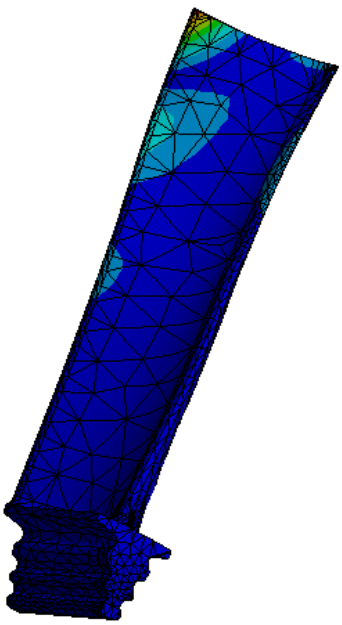

(g) Mode Shape 7 (3213.7 Hz)

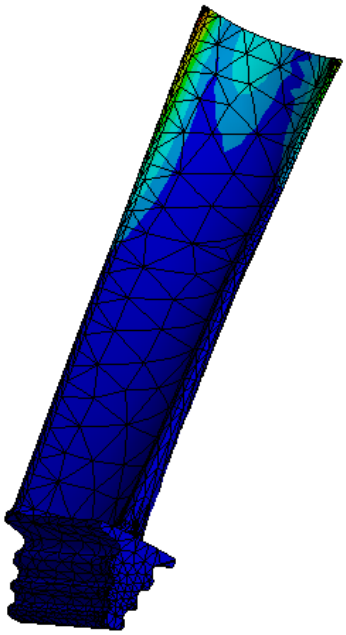

(h) Mode Shape 8 (3851.1Hz)

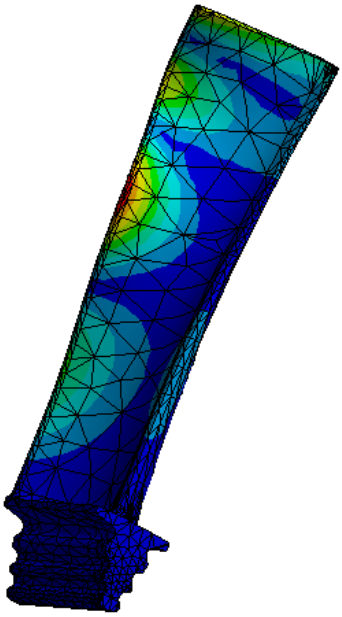

(i) Mode Shape 9 (4193.1 Hz)

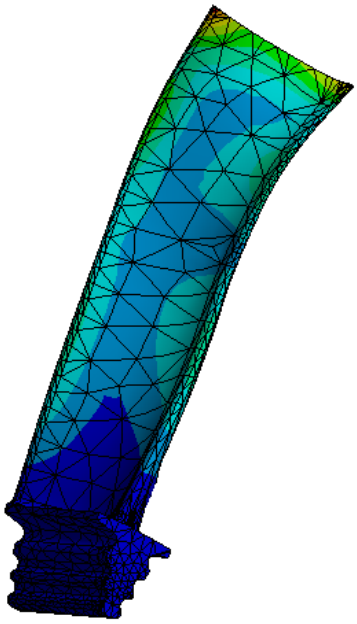

(j) Mode Shape 10 (4420.0 Hz)

Figure 19: Different mode shapes of the DZ125 single crystal blade with their corresponding natural frequencies

Effects of anisotropic crystal orientations:

To analyse the effects of anisotropy i.e. to evaluate variation of frequency caused by different anisotropic angles are plotted in terms of 2D and 3D response charts.

Figure 20 shows the effects of variation of angle φ on natural frequencies and mode shapes of the single crystal blade, where values of angle φ were taken as -15°, -7.5°, 0°, 7.5° and 15°, when θ = 0 and Ψ = 40°. It is found that the frequency variation is found to be maximum with 1.53% variation for 2nd natural frequency (mode shape 2).

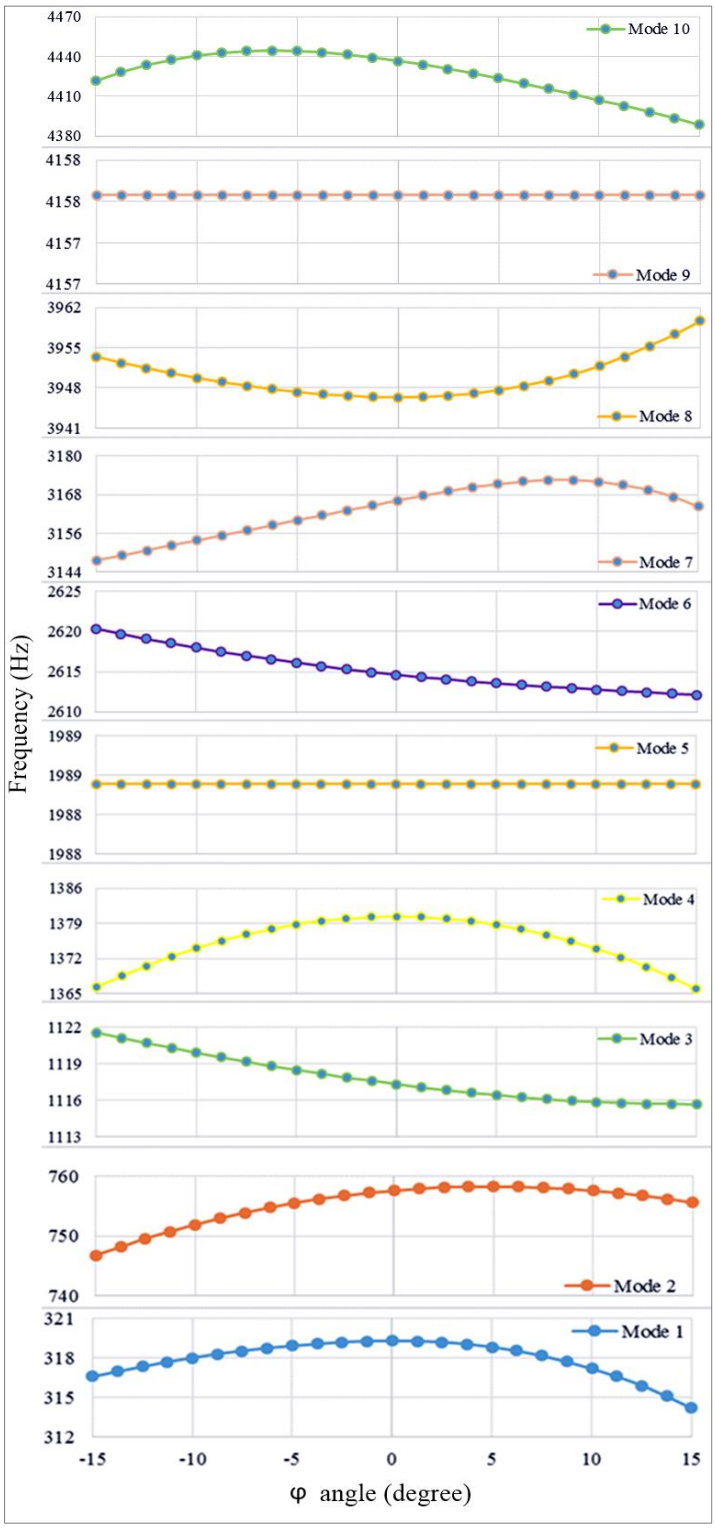

Figure 20: Variation of frequency for different mode shapes when φ (-15° to +15°), Ψ = 40° and θ = 0°

Moreover, frequency variations were calculated for 6 different cases of anisotropic angle orientations and results are plotted in terms of clustered column charts as shown in Figure 21. It is found that the % variation of natural frequencies are ranges from 0.04% (minimum) to 5.3% (maximum).

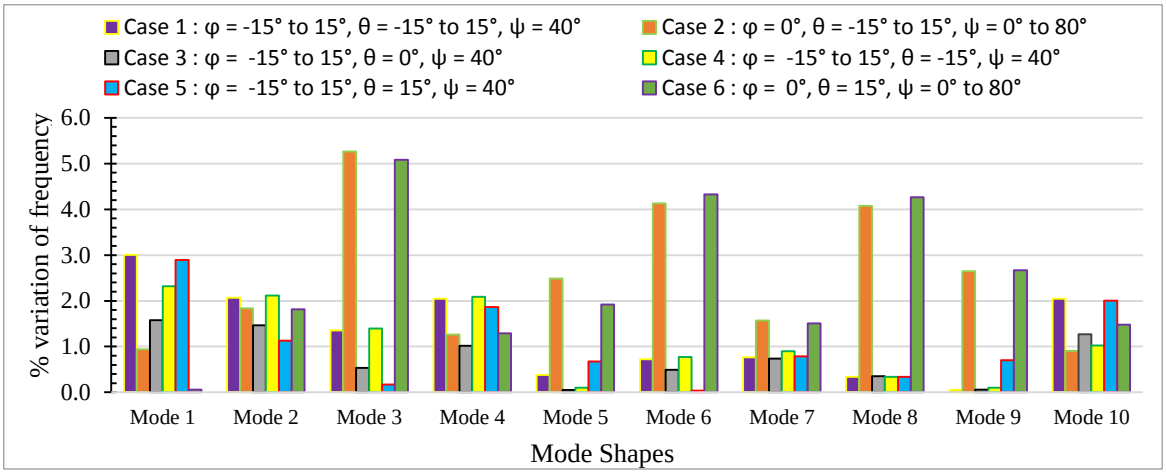

Figure 21: % variation of frequency for different mode shapes with different cases of anisotropy angle orientations

Figure 22 shows the effects of angle θ and φ on 4th natural frequency, taking the values of angle θ as -15^o, -7.5^o, 0^o, 7.5^o and 15^o respectively against φ = -15^o to 15^o, when Ψ = 40^o. In this case, frequency variation is found to be 2.3% for mode 4. From the Figure 22, it is found that the values of natural frequencies are minimum when primary angles are either (φ = -15^o, θ = -15^o) or (φ = 15^o, θ = 15^o).

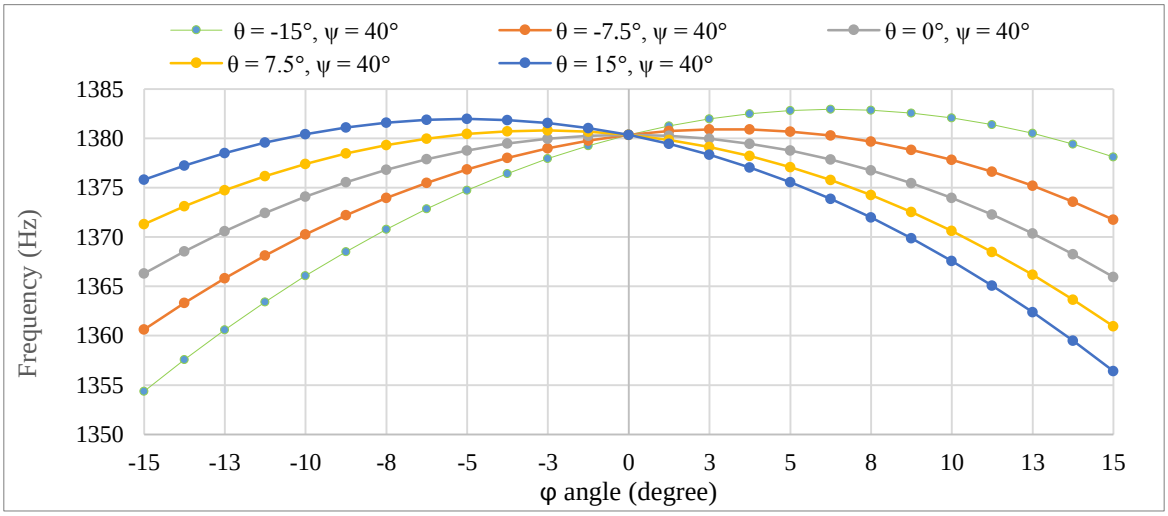

Figure 22: Variation of 4th natural frequency caused by variation of angle θ (-15^o to +15^o) and φ = (-15^o or 15^o), when Ψ = 40^o

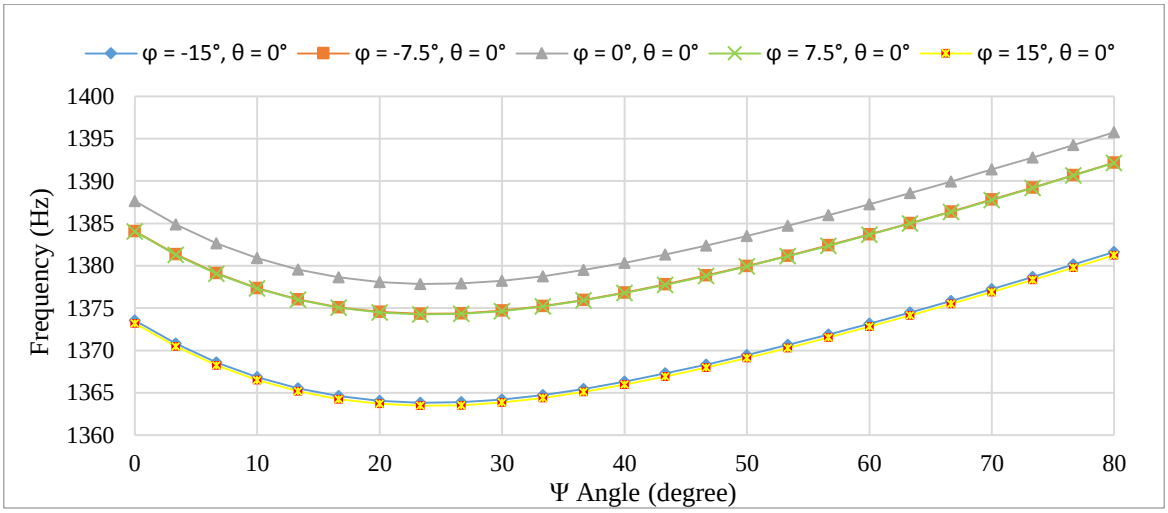

Figure 23: Variation of 4th natural frequency caused by variation of angle φ (-15° to +15°) and Ψ = (0° to 80°), when θ = 0°

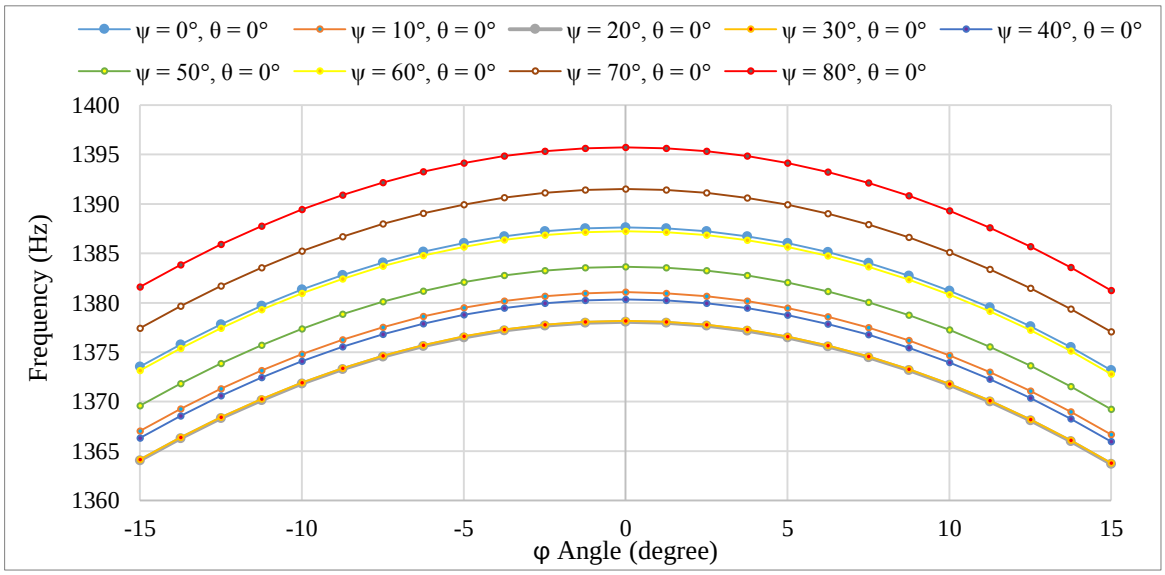

Figure 24: Variation of 4th natural frequency caused by variation of angle Ψ (0° to 80°) and φ (-15° to +15°), when θ= 0°

Figure 23 shows the effects of angle φ and Ψ on 4th natural frequency, where φ values are -15°, -7.5°, 0°, 7.5° and 15° respectively, plotted against Ψ = 0° to 80°, when θ = 0. On the other hand, Figure 24 represents the effects of angle Ψ and φ on 4th natural frequency, when Ψ values are 0°, 10°, 20°, 30°, 40°, 50°, 60°, 70°, and 80° respectively, plotted against φ = -15° to 15° , when θ = 0. From the Figure 23 and Figure 24, it is found that the values of natural frequency are highest when Eulerian angles are at (φ = 0°, θ = 0°, Ψ = 80°) and minimum when the values of Eulerian angles are (φ = -15°, θ = -15°, Ψ ≅ 25°) or (φ = 15°, θ = 15°, Ψ ≅ 25°).

3D response surfaces are also plotted for differed anisotropic angles. Figure 25, Figure 26 and Figure 27 shows the variation of frequency for caused by variation of angle Ψ (0^o to 80^o) and θ (-15^o to $+15^o$), when $\varphi = 0^o$ for mode shapes 2, 4 and 6 respectively. These 3D response surfaces can be compared with the 2D response chart as shown in Figure 23. In these cases, the maximum frequencies are found when $\Psi = 80^o$ and minimum frequencies are recorded somewhere in between $\Psi = 20^o$ to 30^o. Also, frequency variations are found to be 1.8%, 1.3%, 4.1% for mode shapes 2, 4 and 6 respectively.

From this analysis, it is found that for most of the mode shapes viz. 2, 3, 4, 6, 8, 9 and 10, values of frequencies are found to be maximum when secondary angle (Ψ) is at 80^o (3D response charts for all these modes are not presented in this report). The trend of 3D response surfaces of the modes 3, 8, 9 and 10 (which are not presented in this report) are also same as in the cases of mode shape 2, 4 and 6, as shown in Figure 25, Figure 26 and Figure 27 respectively.

Figure 28, Figure 29 and Figure 30 shows the variation of natural frequency caused by the variation of angle φ (-15^o to 15^o) and θ (-15^o to $+15^o$) when $\Psi = 40^o$ for mode shape 1, 2, and 4 respectively. The 3D response surfaces for mode shape 1, 2, and 4 can be compared with the 2D response chart as shown in Figure 22. In these cases, minimum frequencies are recorded when combination of primary angles are either ($\theta = 15^o$, $\varphi = 15^o$) or ($\theta = -15^o$, $\varphi = -15^o$). For rest of the modes (mode shape 3, 5, 7, 8, 9, and 10) results vary from modes to modes (all are not presented in this report). Therefore, in this case there is not any specific value primary angles for maximum and minimum variation of frequency. Although, for most of the cases frequency values are found to be minimum when primary angles are at ($\theta = 15^o$, $\varphi = 15^o$) or ($\theta = -15^o$, $\varphi = -15^o$) as mentioned earlier. In this case frequency variations are found to be 3.0%, 2.1%, and 2.0% for mode shapes 1, 2, and 4 respectively.

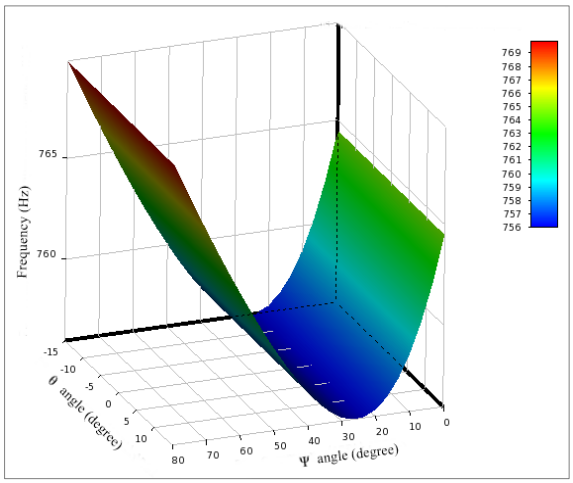

Figure 25: Variation of 2nd natural frequency caused by variation of angle Ψ (0º to 80º) and θ (-15º to +15º), when φ = 0º

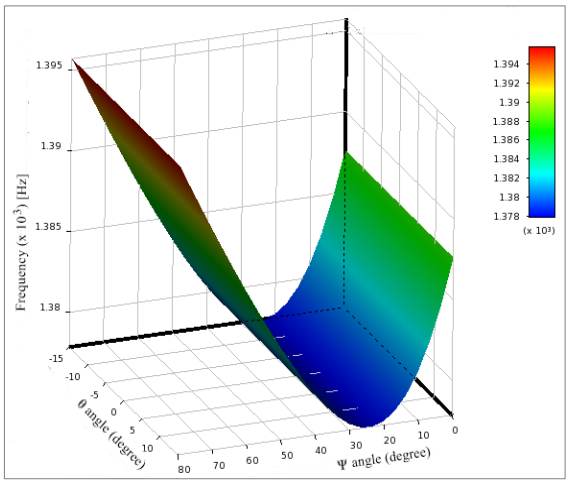

Figure 26: Variation of 4th natural frequency caused by variation of angle Ψ (0º to 80º) and θ (-15º to +15º), when φ = 0º

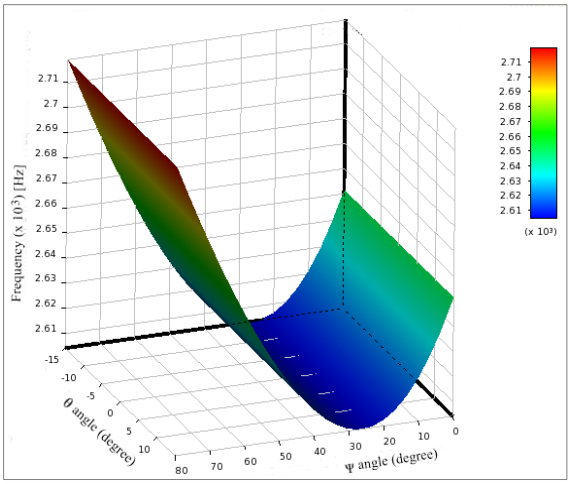

Figure 27: Variation of 6th natural frequency caused by variation of angle Ψ (0º to 80º) and θ (-15º to +15º), when φ = 0º

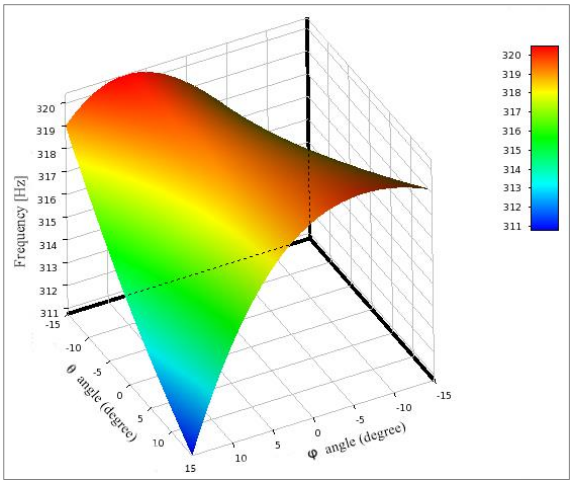

Figure 28: Variation of 1st natural frequency caused by variation of angle φ (-15º to 15º) and θ (-15º to +15º) when Ψ = 40º

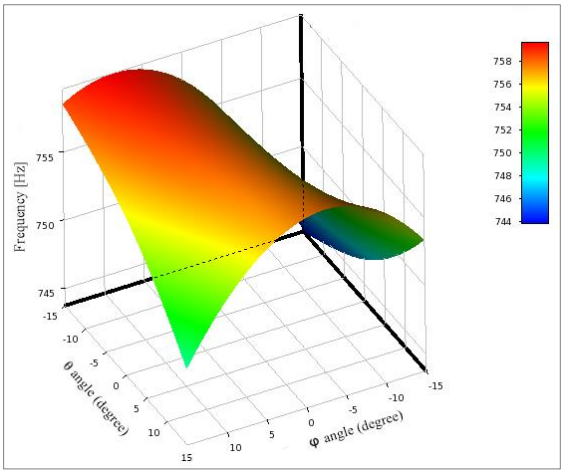

Figure 29: Variation of 2nd natural frequency caused by variation of angle φ (-15º to 15º) and θ (-15º to +15º), when Ψ = 40º

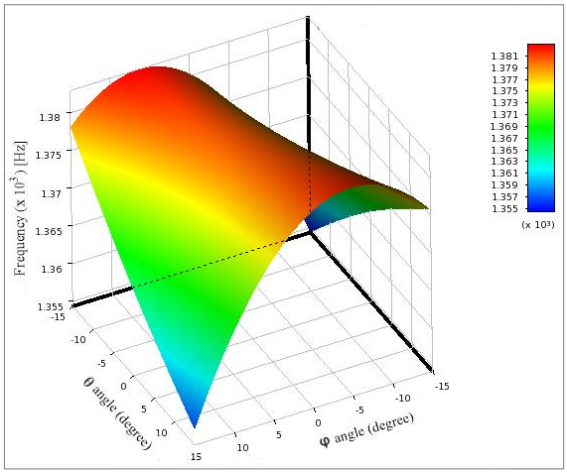

Figure 30: Variation of 4th natural frequency caused by variation of angle φ (-15º to 15º) and θ (-15º to +15º), when Ψ = 40º

4.2 Effects of material anisotropy on modal properties of tuned bladed disc

As per the section 3.5 of chapter 3, modal analysis of a tuned bladed disc blade was carried out with the cyclic symmetry model of a sector for different anisotropic orientations (as mentioned in Table 7 and Table 8) of DZ125 alloy in order to evaluate the effects of material anisotropic orientations on mode shapes and natural frequency of a tuned bladed disc. The results of modal analysis of the original FE model with Eulerian angles ($\varphi = 0°$, $\theta = 0°$, $\psi = 0°$) is tabulated in Table 12; accordingly the nodal diameter versus frequency plot for the tuned bladed disc is plotted Figure 31. Moreover, few selected mode shapes with a nodal diameter corresponding to their corresponding natural frequencies for EO 1 is plotted in the Figure 32.

Table 12: Natural frequencies for different mode shapes with respect to their respective nodal diameters for the original FE model with Eulerian angles ($\varphi = 0$, $\theta = 0$, $\psi = 0$)

ND	Mode 1	Mode 2	Mode 3	Mode 4	Mode 5	Mode 6	Mode 7	Mode 8	Mode 9	Mode 10
0	240	240	280	280	439	439	782	782	1010	1010
1	173	173	326	326	737	737	1053	1053	1231	1231
2	280	280	371	371	779	779	1105	1105	1415	1415
3	310	310	630	630	887	887	1138	1138	1708	1708
4	312	312	699	699	1020	1020	1195	1195	1885	1885
5	312	312	715	715	1059	1059	1249	1249	1902	1902
6	313	313	721	721	1072	1072	1281	1281	1907	1907
7	313	313	724	724	1078	1078	1300	1300	1910	1910
8	313	313	726	726	1081	1081	1311	1311	1912	1912
9	313	313	727	727	1083	1083	1319	1319	1913	1913
10	313	313	728	728	1084	1084	1324	1324	1914	1914
11	313	313	728	728	1085	1085	1328	1328	1915	1915
12	313	313	729	729	1085	1085	1330	1330	1916	1916
13	313	313	729	729	1086	1086	1332	1332	1916	1916
14	313	313	729	729	1086	1086	1333	1333	1916	1916
15	313	313	729	729	1086	1086	1333	1333	1916	1916

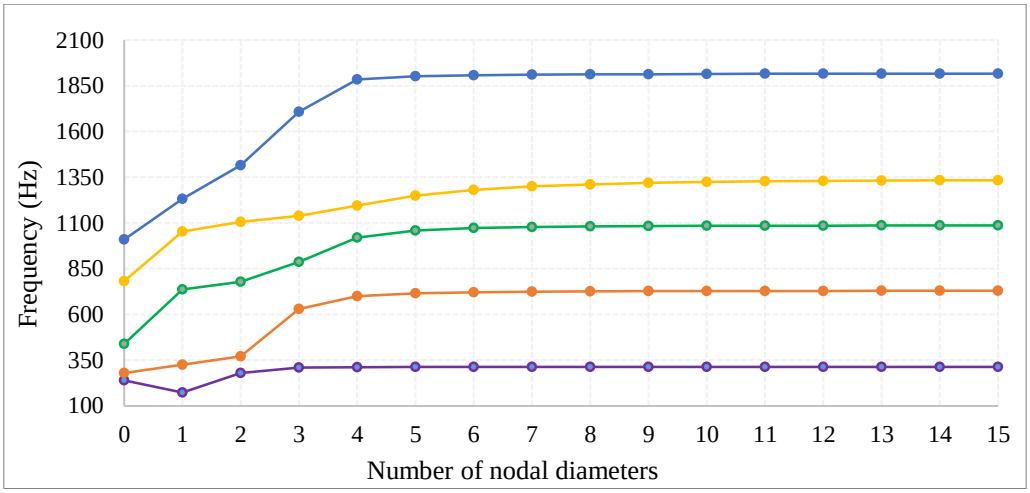

Figure 31: Natural frequencies vs. number of nodal diameters for the tuned bladed disc with cyclic symmetry

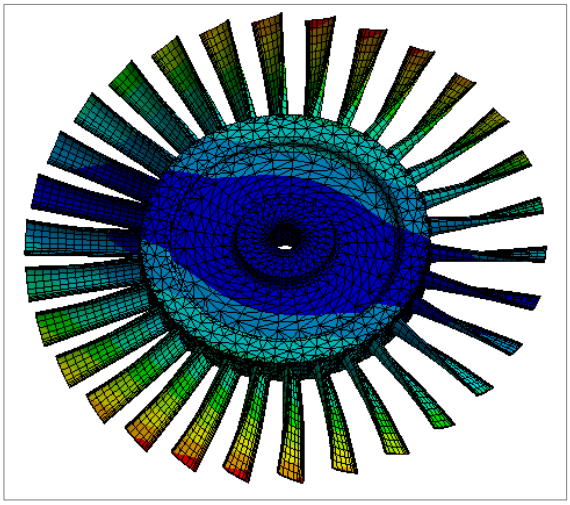

(a) Mode Shape 1, ND 1 (173 Hz)

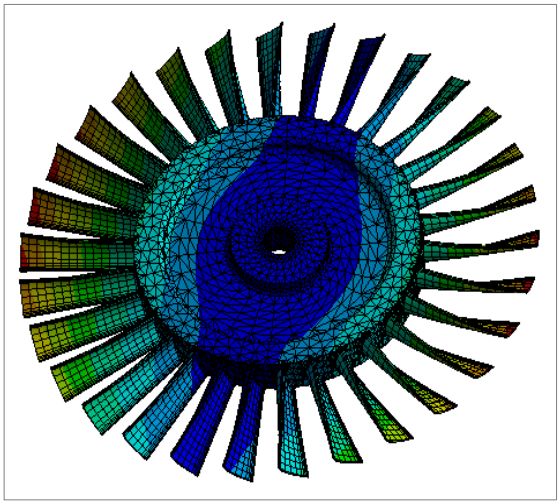

(b) Mode Shape 2, ND 1 (173 Hz)

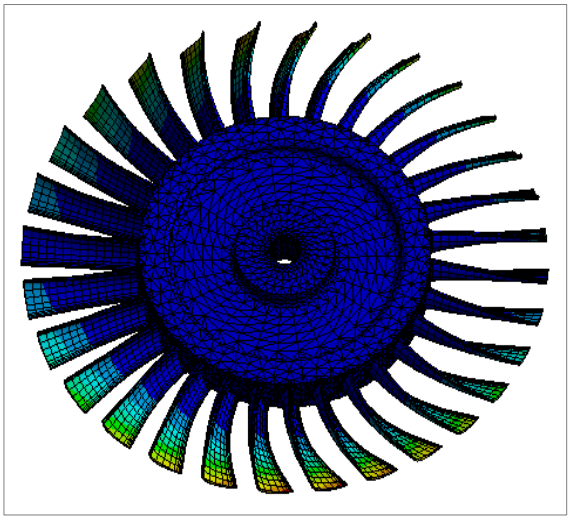

(d) Mode Shape 3, ND 1 (326 Hz)

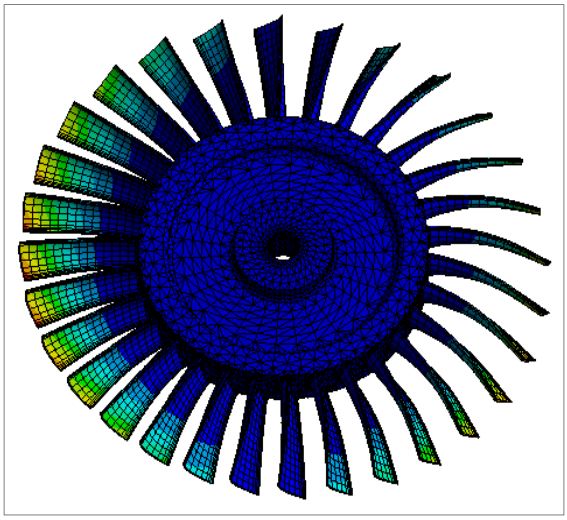

(e) Mode Shape 4, ND 1 (326 Hz)

Figure 32: Different mode shapes of the tuned bladed disc with their corresponding natural frequencies for ND 1

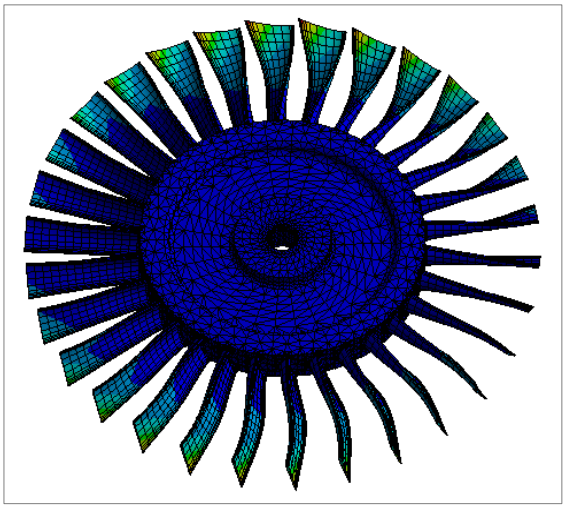

(d) Mode Shape 5, ND 1 (737 Hz)

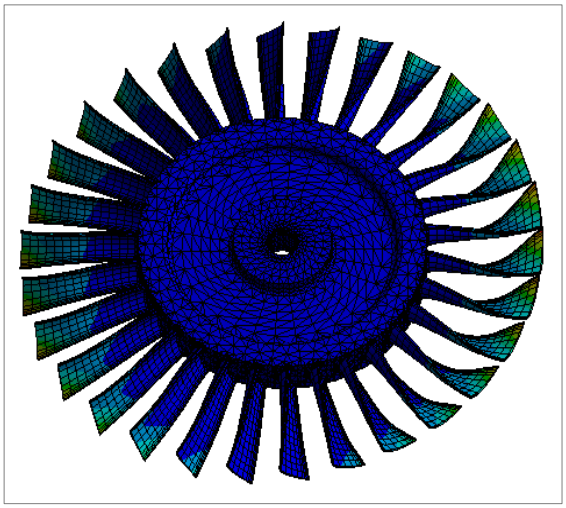

(e) Mode Shape 6, ND 1 (737 Hz)

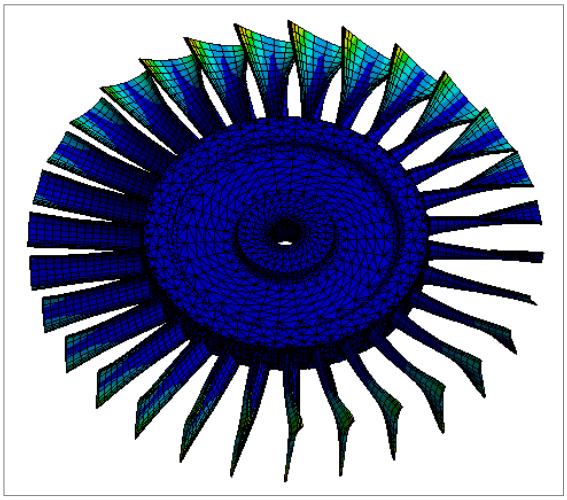

(f) Mode Shape 7, ND 1 (1053 Hz)

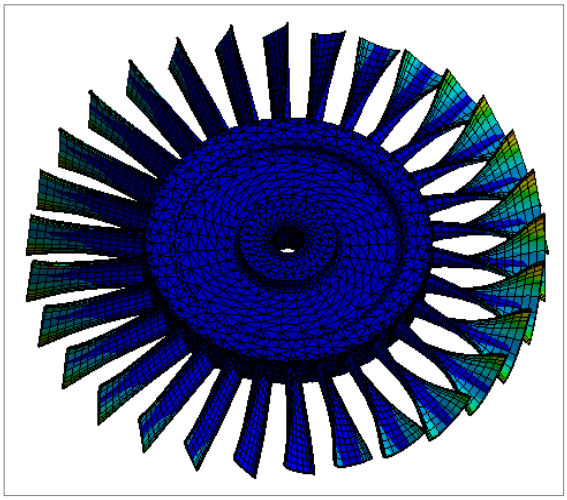

(g) Mode Shape 8, ND 1 (1053 Hz)

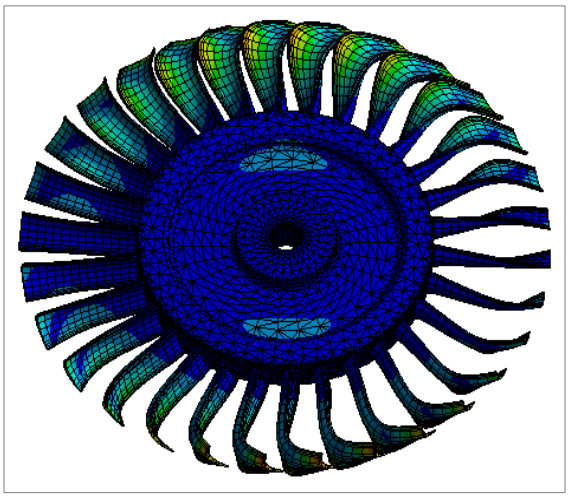

(h) Mode Shape 9, ND 1 (1231 Hz)

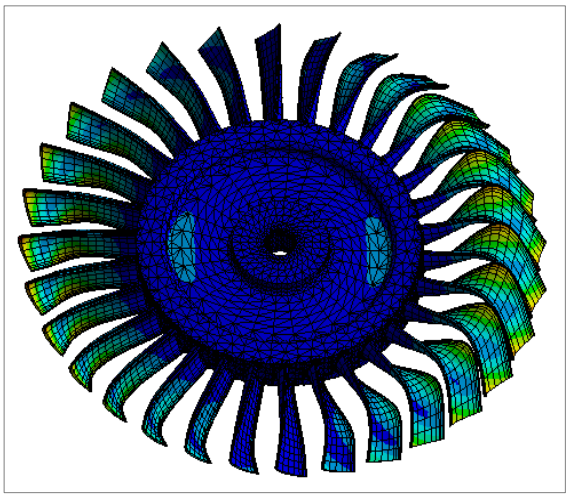

(i) Mode Shape 10, ND 1 (1231 Hz)

Figure 32 : Different mode shapes of the tuned bladed disc with their corresponding natural frequencies for ND 1

Effects of anisotropic crystal orientations:

Variation of the natural frequency with their corresponding mode shapes for different nodal diameters are plotted from the Figure 34 to Figure 48. It can be seen from the Figure 34 to Figure 38 that the values natural frequencies are minimum when primary angles are at ($\varphi = 15^o$, $\theta = 15^o$) or ($\varphi = -15^o$, $\theta = -15^o$). On the other hand, Figure 39 to Figure 47 shows that the values natural frequencies are found to be maximum when secondary angle, $\Psi = 80^o$ and minimum frequencies are recorded somewhere in between $\Psi = 20^o$ to 30^o. Moreover, it is evident form the Figure 44 to Figure 47 that, values natural frequencies are found to be maximum when ($\varphi = 0^o$, $\theta = 0^o$, $\Psi = 80^o$).

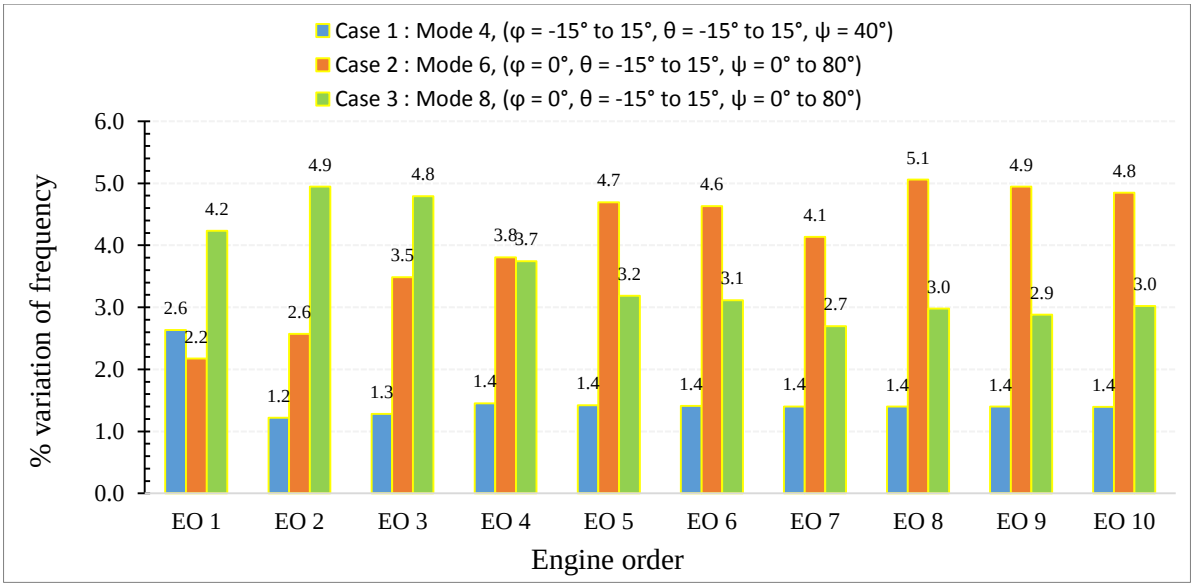

Figure 33: % variation of frequency for different mode shapes for their corresponding engine orders with different cases of anisotropy angle orientations for tuned bladed disc

Variation of natural frequency due to anisotropic material orientations were calculated for 3 different cases of anisotropic angle orientations with different mode shapes and engine-orders, and results plotted in terms of clustered column charts as shown in Figure 33. From these investigated cases, it is found that the values of % variation of natural frequencies are ranges from 1.2% (minimum) to 5.1% (maximum).

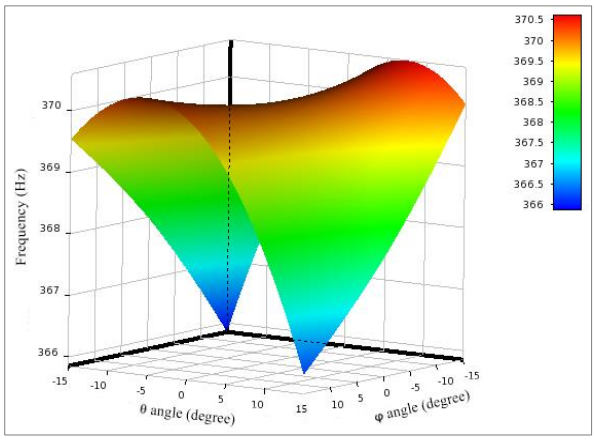

Figure 34: Variation of 4th natural frequency caused by variation of angle φ (-15º to 15º) and θ (-15º to +15º), when Ψ = 40º for ND 2

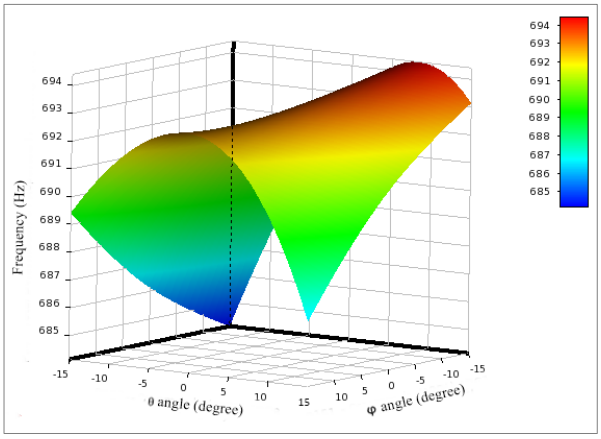

Figure 35: Variation of 4th natural frequency caused by variation of angle φ (-15º to 15º) and θ (-15º to +15º), when Ψ = 40º for ND 4

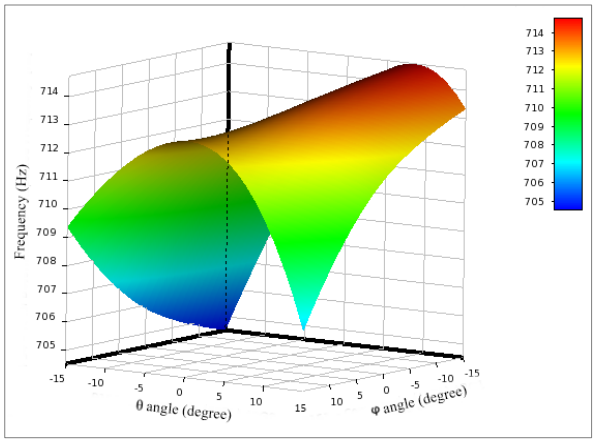

Figure 36: Variation of 4th natural frequency caused by variation of angle φ (-15º to 15º) and θ (-15º to +15º), when Ψ = 40º for ND 6

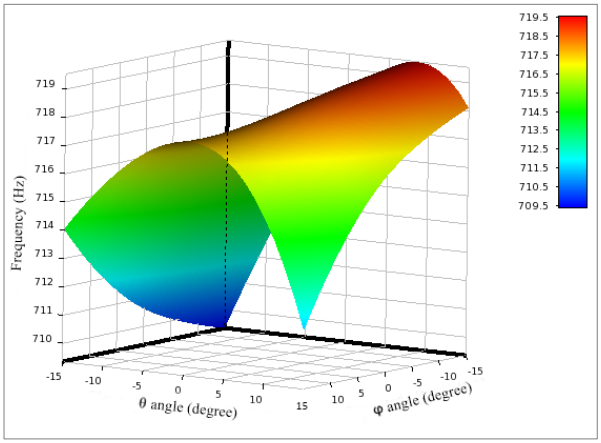

Figure 37: Variation of 4th natural frequency caused by variation of angle φ (-15º to 15º) and θ (-15º to +15º), when Ψ = 40º for ND 8

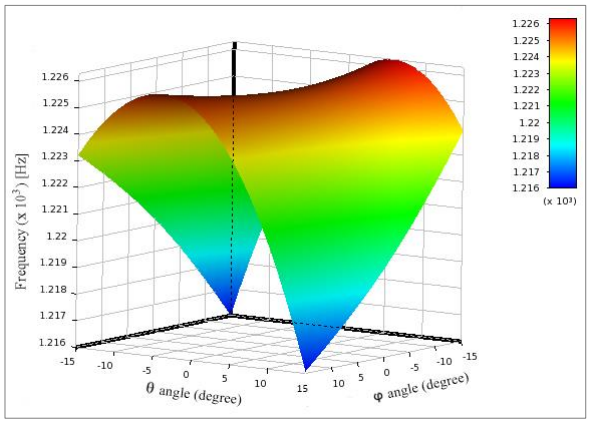

Figure 38: Variation of 4th natural frequency caused by variation of angle φ (-15º to 15º) and θ (-15º to +15º), when Ψ = 40º for ND 10

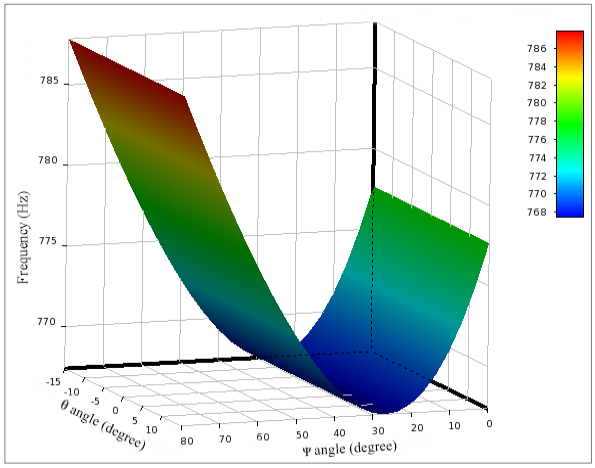

Figure 39: Variation of 6th natural frequency caused by variation of angle Ψ (0º to 80º) and θ (-15º to 15º), when φ = 0º for ND 2

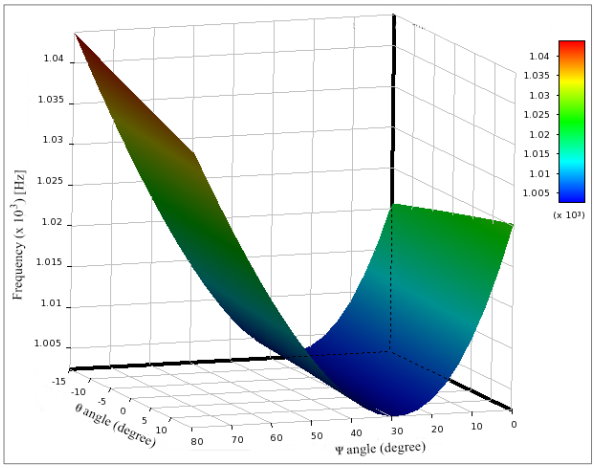

Figure 40: Variation of 6th natural frequency caused by variation of angle Ψ (0º to 80º) and θ (-15º to 15º), when φ = 0º for ND 4

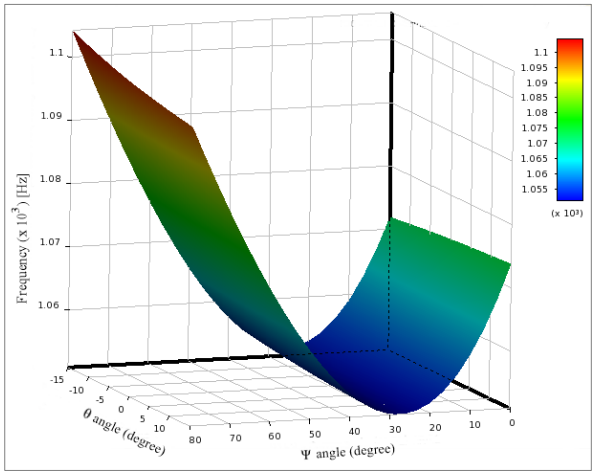

Figure 41: Variation of 6th natural frequency caused by variation of angle Ψ (0º to 80º) and θ (-15º to 15º), when φ = 0º for ND 6

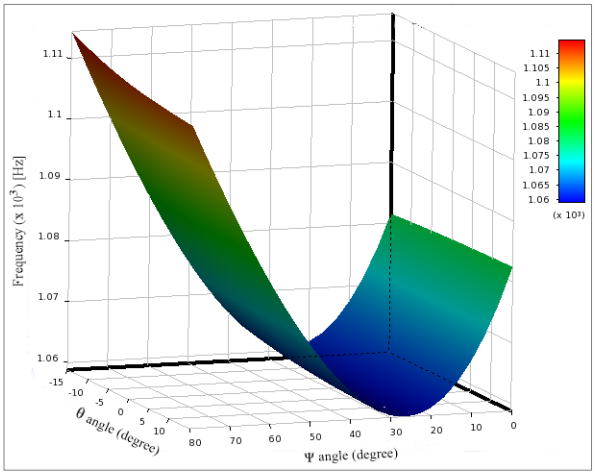

Figure 42: Variation of 6th natural frequency caused by variation of angle Ψ (0º to 80º) and θ (-15º to 15º), when φ = 0º for ND 8

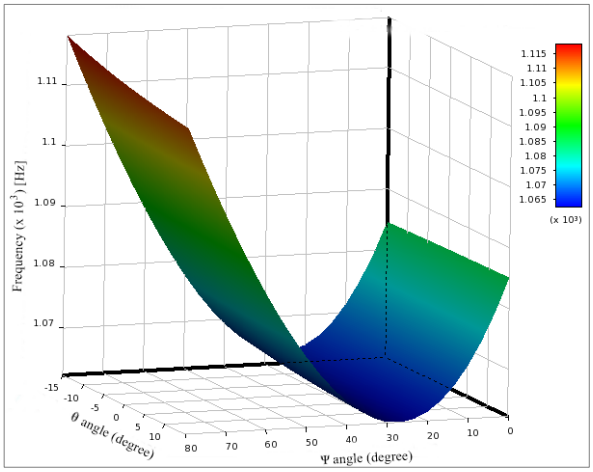

Figure 43: Variation of 6th natural frequency caused by variation of angle Ψ (0º to 80º) and θ (-15º to 15º), when φ = 0º for ND 10

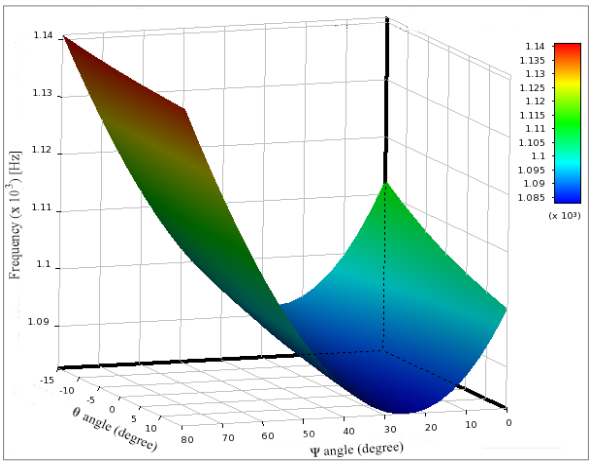

Figure 44: Variation of 8th natural frequency caused by variation of angle Ψ (0º to 80º) and θ (-15º to 15º), when φ = 0º for ND 2

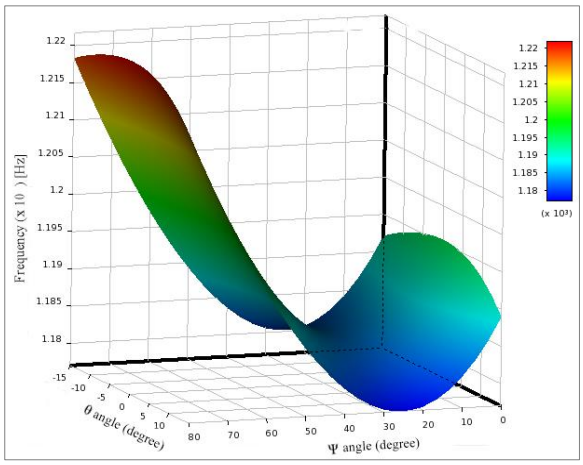

Figure 45: Variation of 8th natural frequency caused by variation of angle Ψ (0º to 80º) and θ (-15º to 15º), when φ = 0º for ND 4

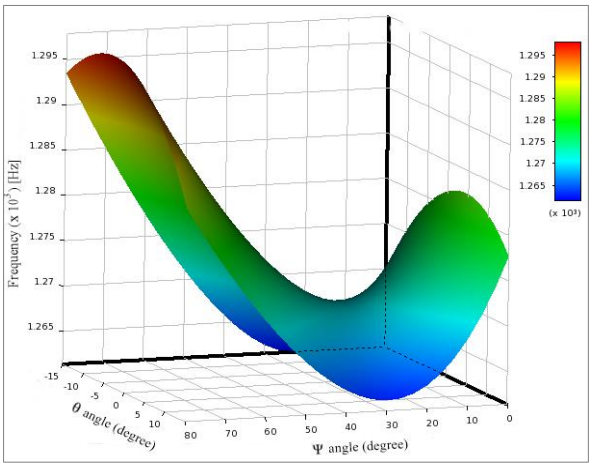

Figure 46: Variation of 8th natural frequency caused by variation of angle Ψ (0º to 80º) and θ (-15º to 15º), when φ = 0º for ND 6

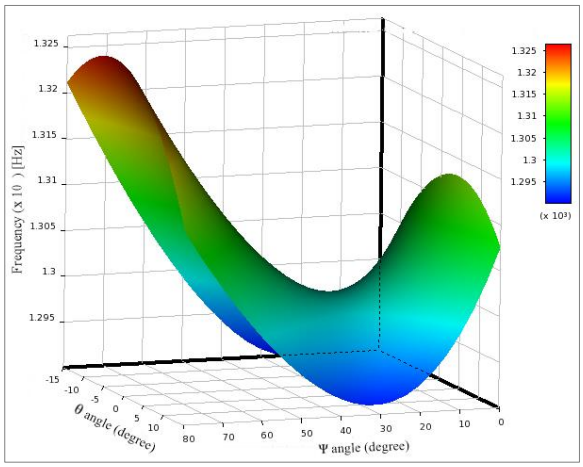

Figure 47: Variation of 8th natural frequency caused by variation of angle Ψ (0º to 80º) and θ (-15º to 15º), when φ = 0º for ND 8

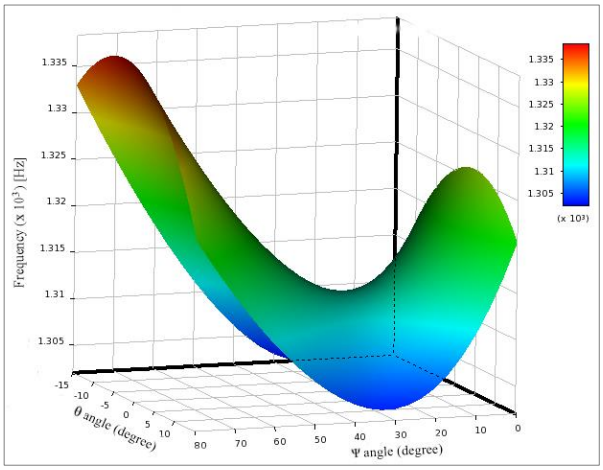

Figure 48: Variation of 8th natural frequency caused by variation of angle Ψ (0º to 80º) and θ (-15º to 15º), when φ = 0º for ND 10

4.3 Effects of material anisotropy on forced response and modal properties of mistuned bladed disc

In order to evaluate the effects of material anisotropic orientations on forced response and modal properties of mistuned bladed disc, the forced response harmonic analysis was carried out for mistuned bladed disc as per the section 3.6 of chapter 3, with four mistuning patterns as tabulated in Table 10. On the other hand, harmonic analysis of the tuned bladed disc was carried out with Eulerian angles ($\varphi = 0, \theta = 0, \psi = 0$). Analysis for both tuned and mistuned bladed disc were carried out for EO 2 and EO 4 as shown in Figure 49.

Forced response of the tuned bladed disc with Eulerian angles ($\varphi = 0, \theta = 0, \psi = 0$) for EO 2 and EO 4 is presented in Figure 50. Forced responses of the mistuned bladed disc for EO 2 and EO 4 is plotted in Figure 51 and Figure 52. Forced responses for both tuned and mistuned bladed disc were calculated for 150 modes (0 Hz to 2000 Hz).

Afterwards, close view of peak frequency responses for both tuned and mistuned bladed discs are plotted with four mistuning patterns (mistuning pattern 1, 2, 3 and 4 as mentioned in Table 10). Variation of peak responses with different mistuning patterns can be observed from these plots.

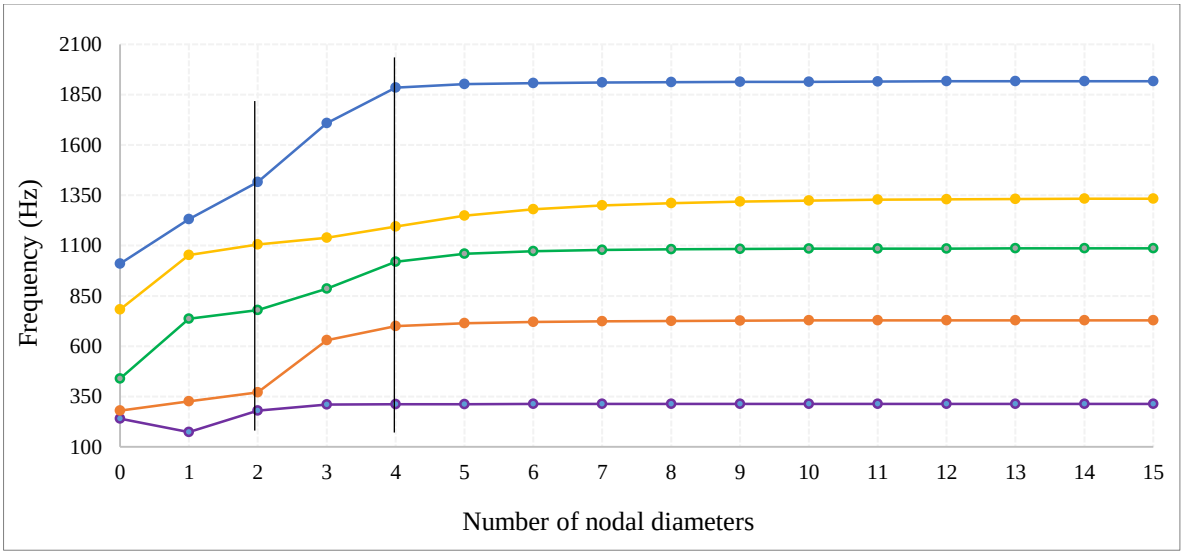

Figure 49 : Natural frequencies vs. number of nodal diameters showing ND 2 and ND 4 for which forced responses were calculated

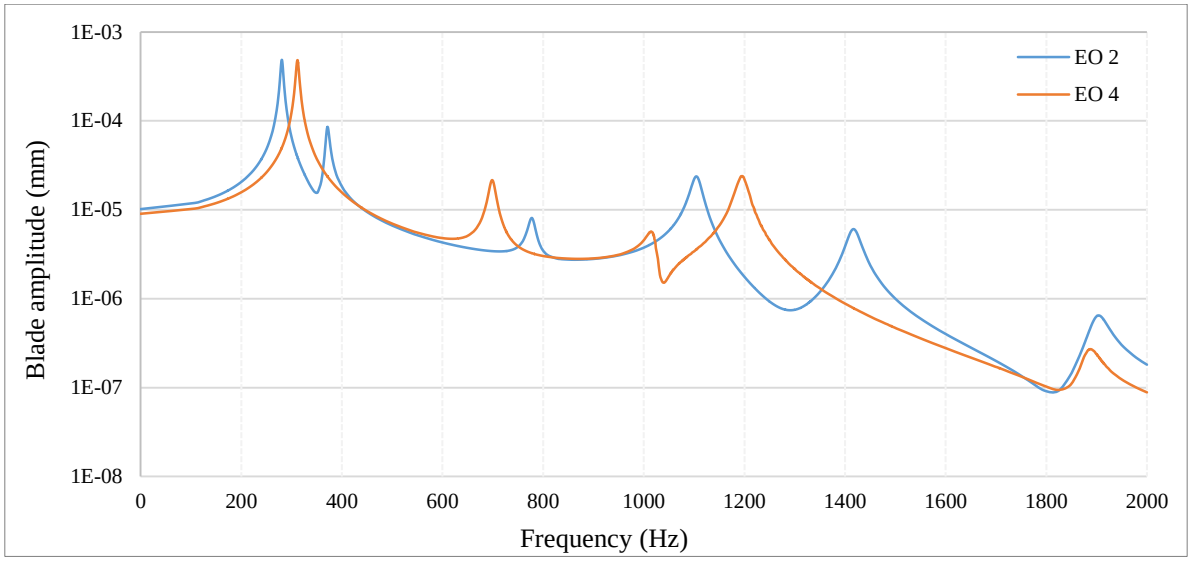

Figure 50: Forced responses of tuned bladed disc with EO 2 and EO 4

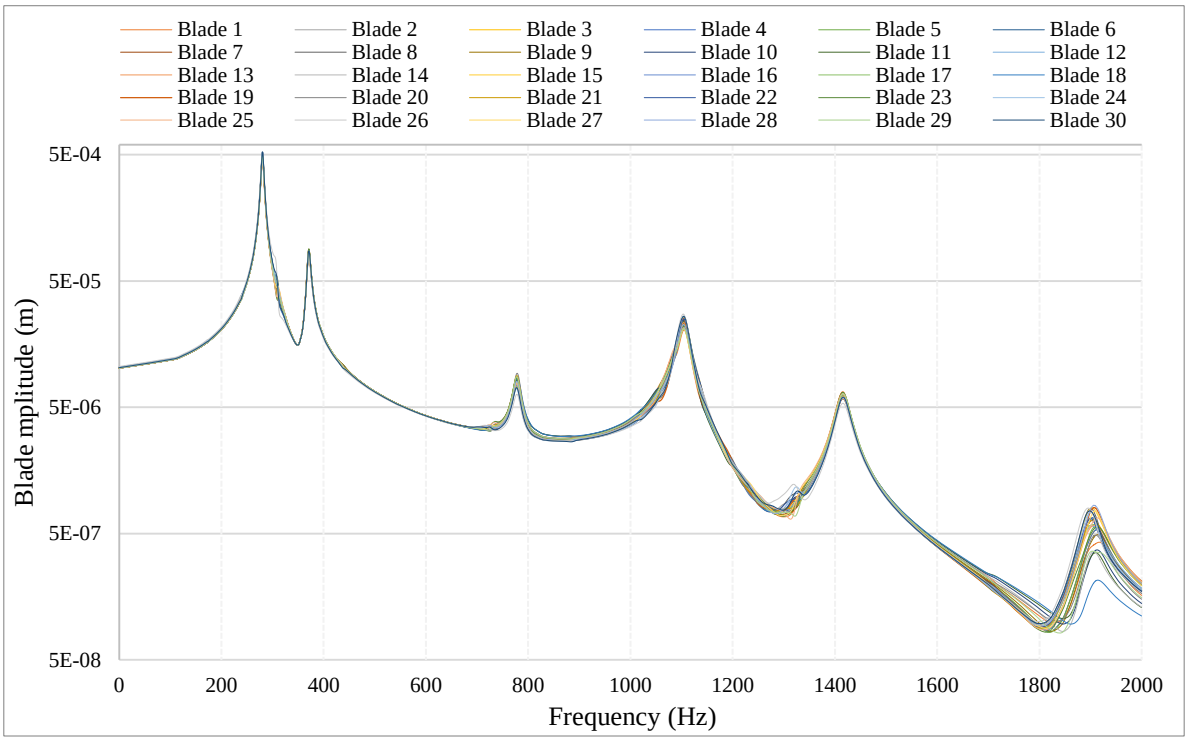

Figure 51 : Forced responses of mistuned bladed disc with EO 2

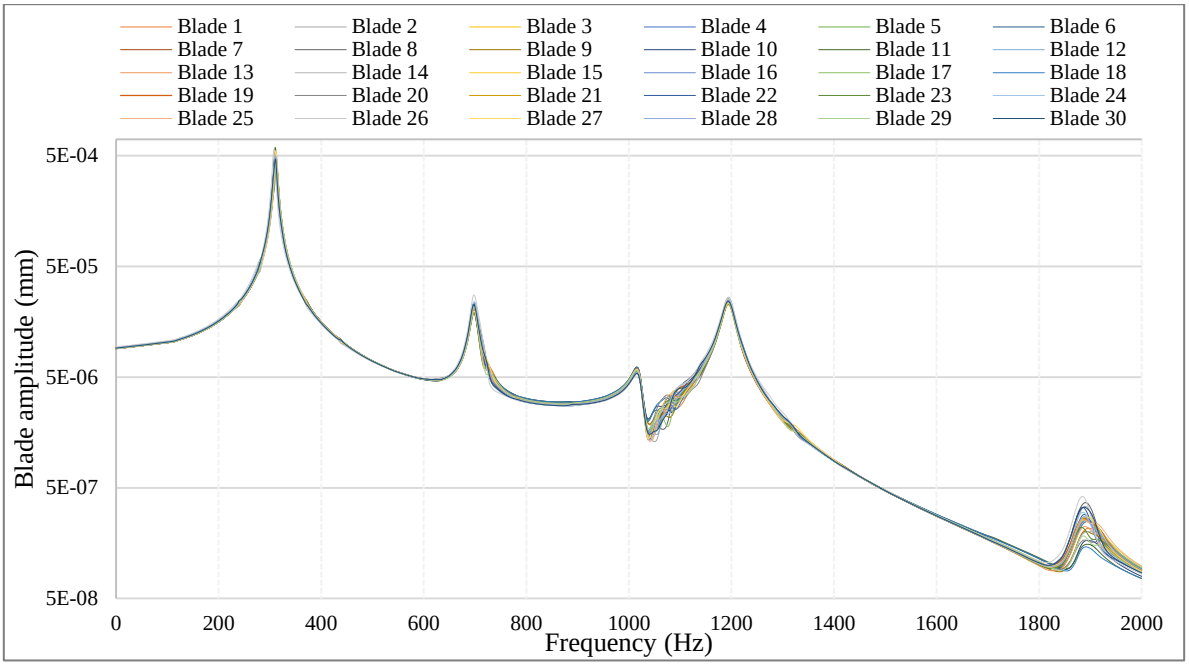

Figure 52 : Forced responses of mistuned bladed disc with EO 4

Blade amplitude vs. frequency plots for the 1st resonance frequency range (275 Hz to 287 Hz) at EO 2 are plotted for mistuning pattern 1, 2, 3 and 4, in Figure 53, Figure 54, Figure 55 and Figure 56 respectively. Also, blade amplitude vs. frequency plots for the 2nd resonance frequency range (364 Hz to 380 Hz) at EO 2 are plotted for mistuning pattern 1, 2, 3 and 4, in Figure 57, Figure 58, Figure 59, and Figure 60 respectively. Moreover, blade amplitude vs. frequency plots for 1st resonance frequency range (292 Hz to 327 Hz) at EO 4 are plotted for mistuning pattern 1, 2, 3 and 4, in the Figure 61 Figure 62 Figure 63 and Figure 64 respectively.

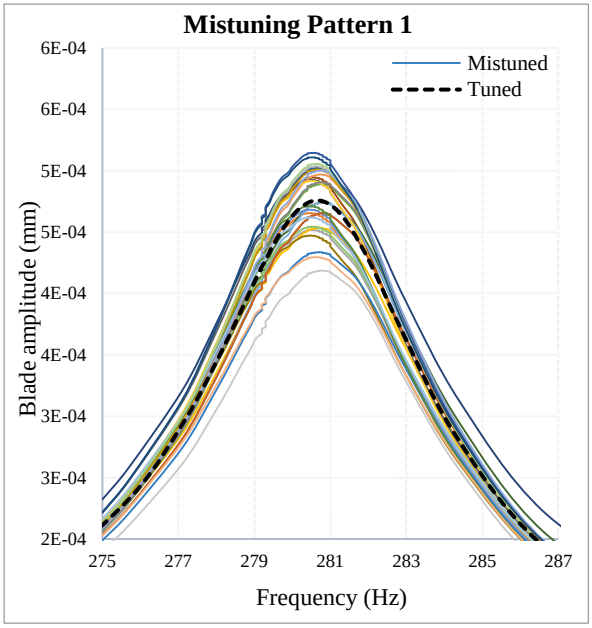

Figure 53: Blade amplitude vs. frequency for the 1st resonance frequency with mistuning pattern 1 & EO 2, (275 Hz to 287 Hz)

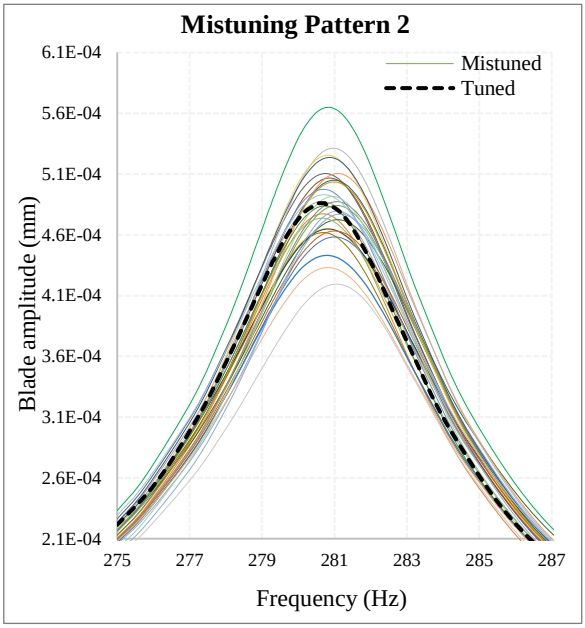

Figure 54: Blade amplitude vs. frequency for the 1st resonance frequency with mistuning pattern 2 & EO 2, (275 Hz to 287 Hz)

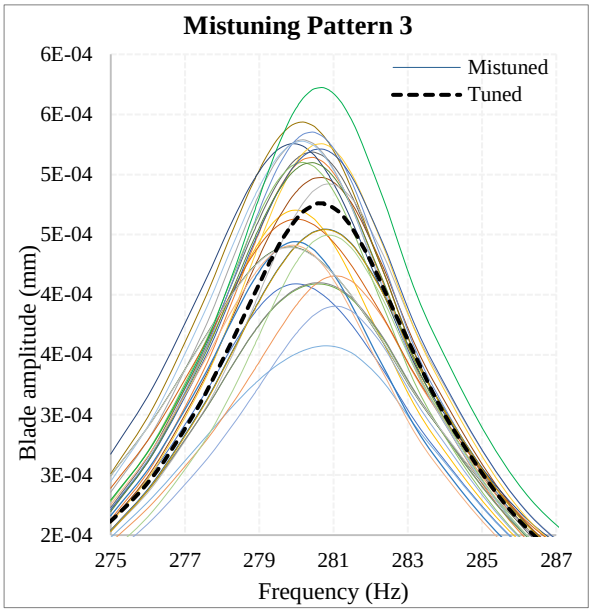

Figure 55: Blade amplitude vs. frequency for the 1st resonance frequency with mistuning pattern 3 & EO 2, (275 Hz to 287 Hz)

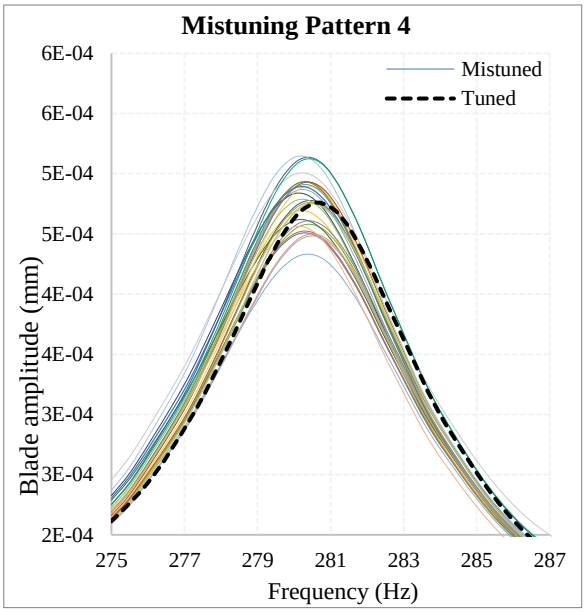

Figure 56: Blade amplitude vs. Frequency for the 1st resonance frequency with mistuning pattern 4 & EO 2, (275 Hz to 287 Hz)

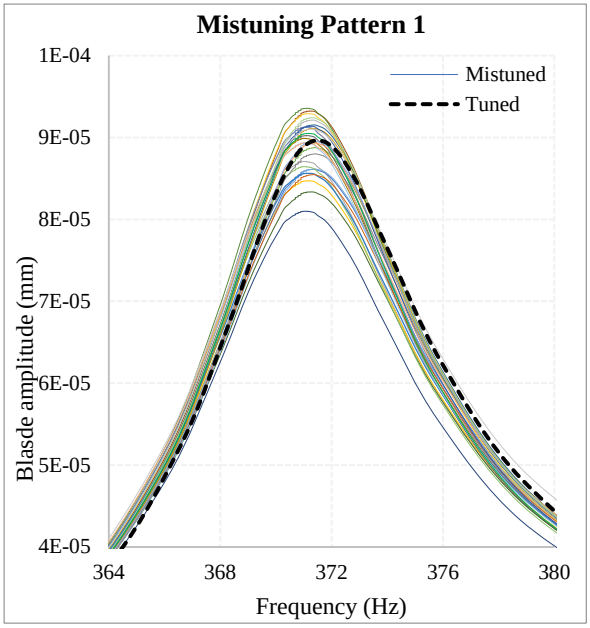

Figure 57: Blade amplitude vs. frequency for the 2nd resonance frequency with mistuning pattern 1 & EO 2, (364 Hz to 380 Hz)

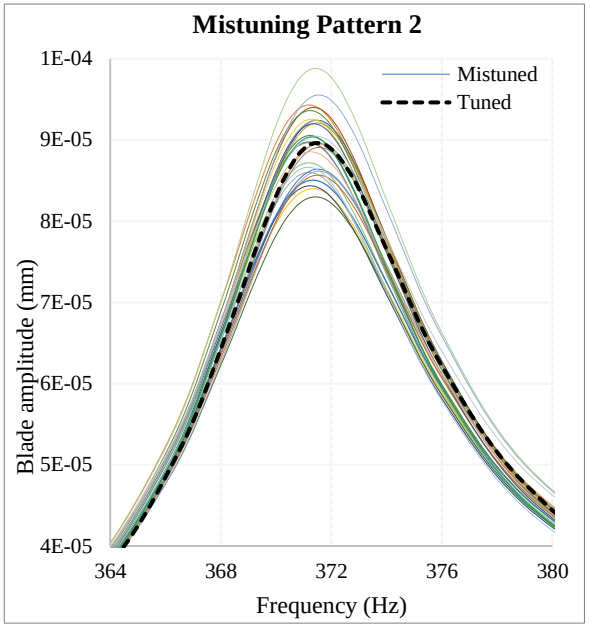

Figure 58: Blade amplitude vs. frequency for the 2nd resonance frequency with mistuning pattern 2 & EO 2, (364 Hz to 380 Hz)

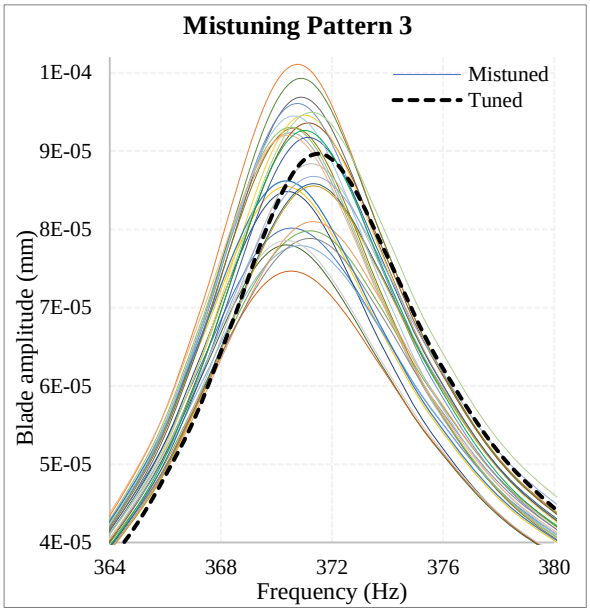

Figure 59: Blade amplitude vs. frequency for the 2nd resonance frequency with mistuning pattern 3 & EO 2, (364 Hz to 380 Hz)

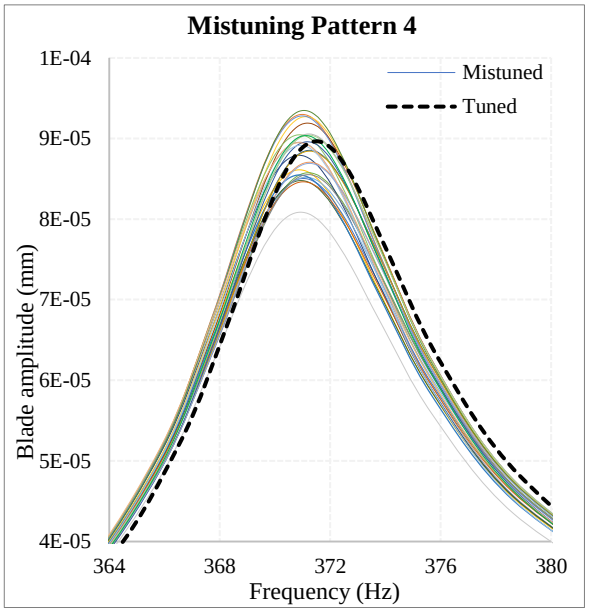

Figure 60: Blade amplitude vs. frequency for the 2nd resonance frequency with mistuning pattern 4 & EO 2, (364 Hz to 380 Hz)

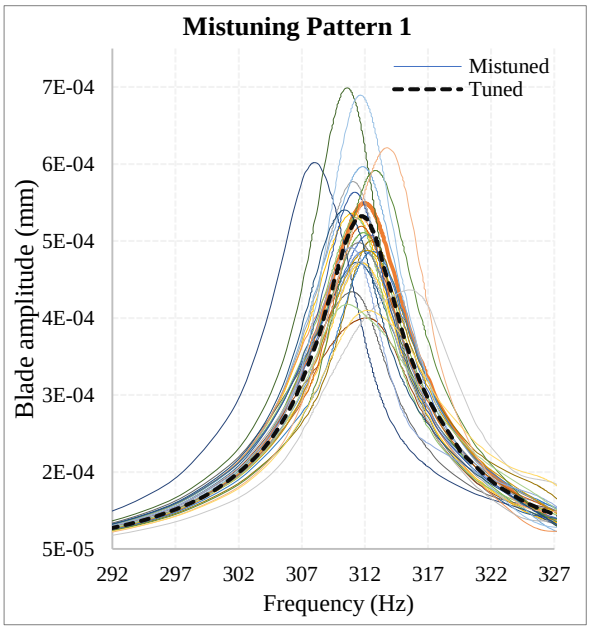

Figure 61: Blade amplitude vs. frequency for the 1st resonance frequency with mistuning pattern 1 & EO 4, (292 Hz to 327 Hz)

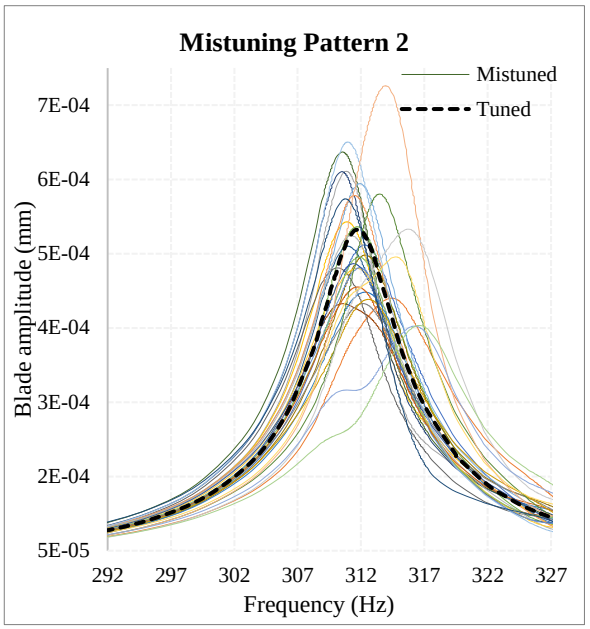

Figure 62: Blade amplitude vs. frequency for the 1st resonance frequency with mistuning pattern 2 & EO 4, (292 Hz to 327 Hz)

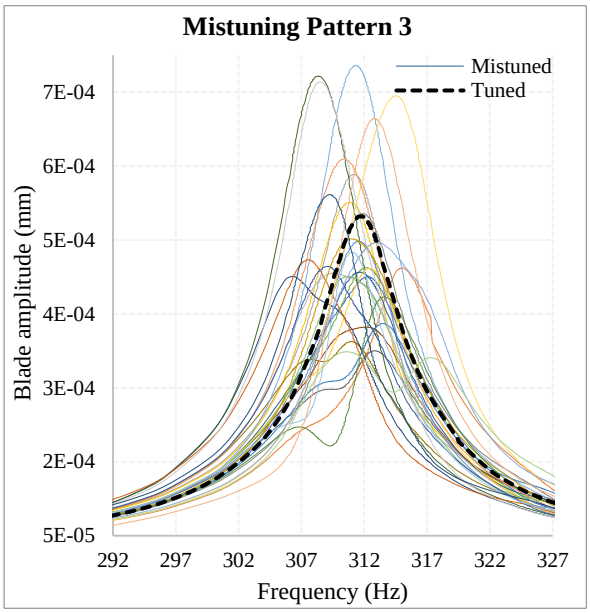

Figure 63: Blade amplitude vs. frequency for the 1st resonance frequency with mistuning pattern 3 & EO 4, (292 Hz to 327 Hz)

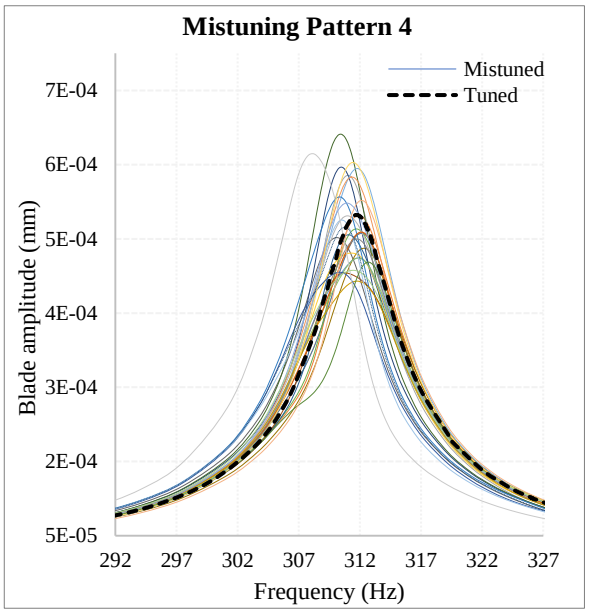

Figure 64: Blade amplitude vs. frequency for the 1st resonance frequency with mistuning pattern 4 & EO 4, (292 Hz to 327 Hz)

Effects of anisotropic orientation on amplification factor:

The effects of the mistuning (due to the anisotropic material orientation of DZ125 blades) on amplification factors or normalised response are demonstrated in Figure 65, Figure 66 and Figure 67. The maximum normalised response or amplification factor is defined as a ratio of the maximum amplitude of a mistuned bladed disk, found in the frequency range of interest, to the maximum amplitude of a tuned bladed disk [48].

In this study, distributions of the maximum normalised amplitudes were calculated for each blade of the mistuned bladed disk with four different mistuning patterns (mistuning pattern 1, 2, 3 and 4) are plotted from the Figure 65 Figure 66 and Figure 67.

In Figure 65, maximum normalised forced responses are plotted against number of blades for EO 2 in the 1st resonance frequency range (275 Hz to 287 Hz); where normalised responses are found to be in the range of (0.91 to 1.12), (0.88 to 1.10), (0.80 to 1.27) and (0.86 to 1.10) for mistuning pattern 1, 2, 3, and 4 respectively. Figure 66 shows the maximum normalised forced responses versus number of blades for EO 2 in the 2nd resonance frequency range (364 Hz to 380 Hz); in this case normalised responses are found to be in the range of (0.90 to 1.04), (0.91 to 1.05), (0.85 to 1.13) and (0.90 to 1.06) for mistuning pattern 1, 2, 3, and 4 respectively. Lastly, Figure 67 represents the maximum normalised forced responses versus number of blades for EO 4 in the 1st resonance frequency range (292 Hz to 327 Hz); where normalised forced responses are found to be in the range of (0.68 to 1.33), (0.66 to 1.85), (0.64 to 1.76) and (0.82 to 1.25) for mistuning pattern 1, 2, 3, and 4 respectively.

The values of the maximum normalised amplitudes found among all blades of the assembly with four different mistuning patterns are plotted in Figure 68.

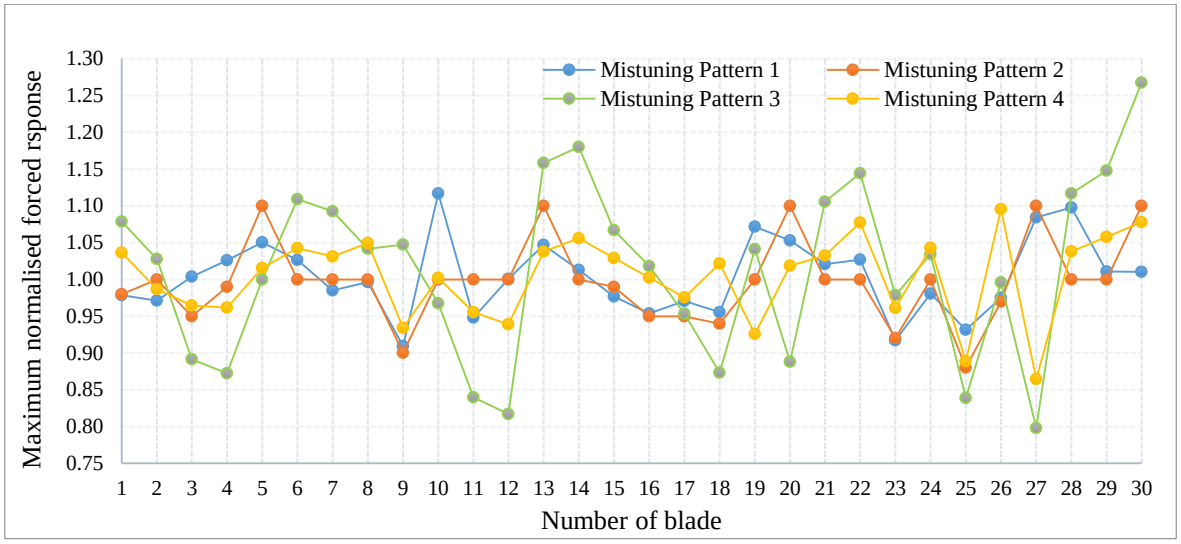

Figure 65: Maximum normalised forced response vs. number of blades for 1st resonance frequency range, EO 2, (275 Hz to 287 Hz)

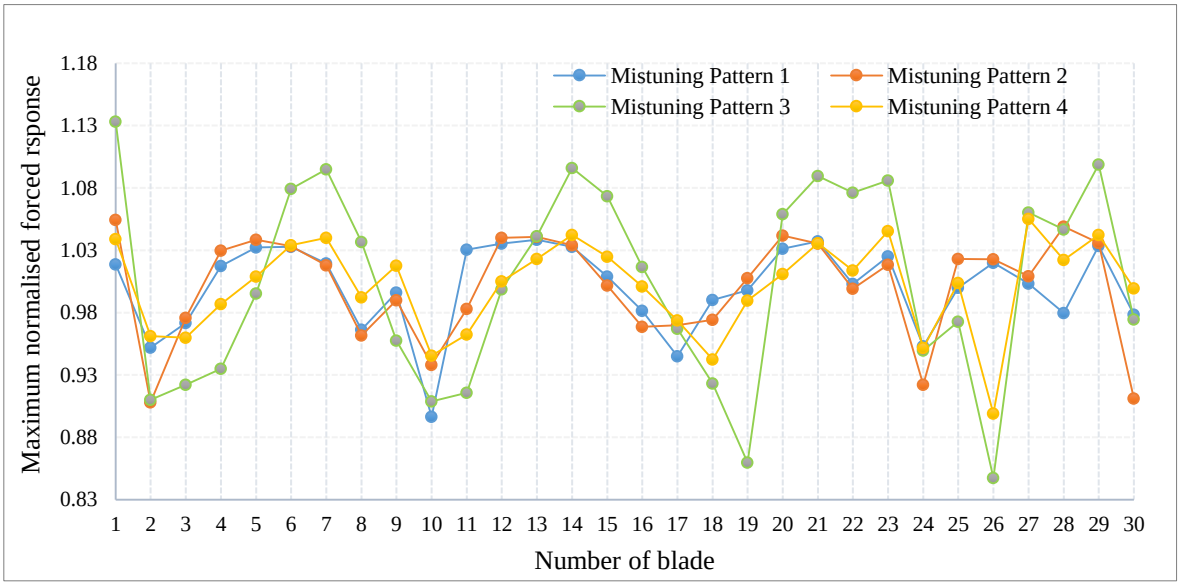

Figure 66: Maximum normalised forced response vs. number of blades for 2nd resonance frequency range, EO 2, (364 Hz to 380 Hz)

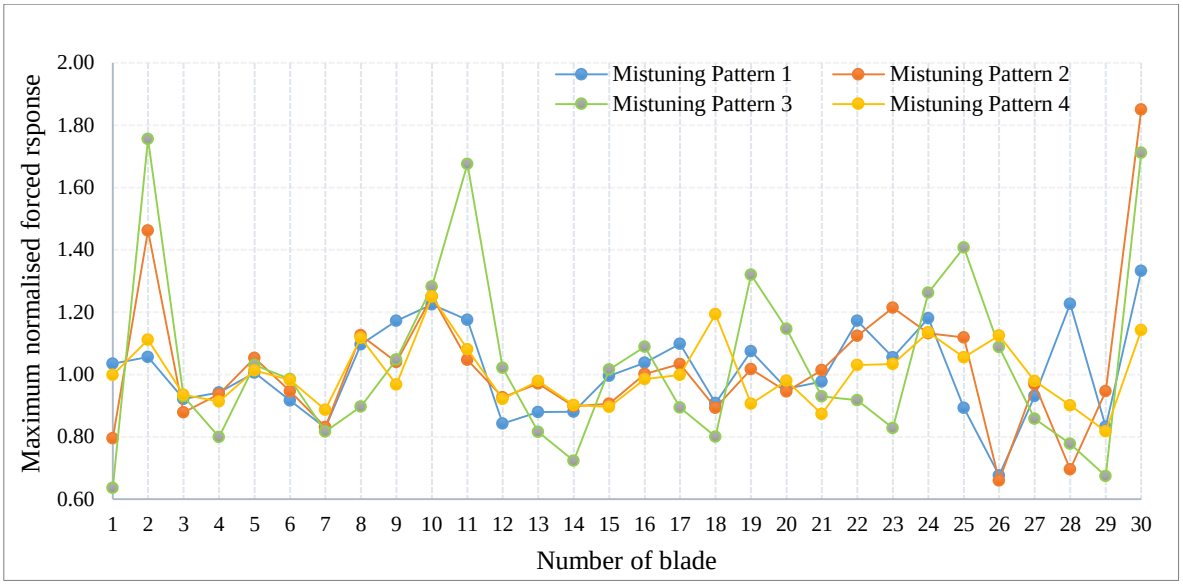

Figure 67: Maximum normalised forced response vs. number of blades for 1st resonance frequency range, EO 4, (292 Hz to 327 Hz)

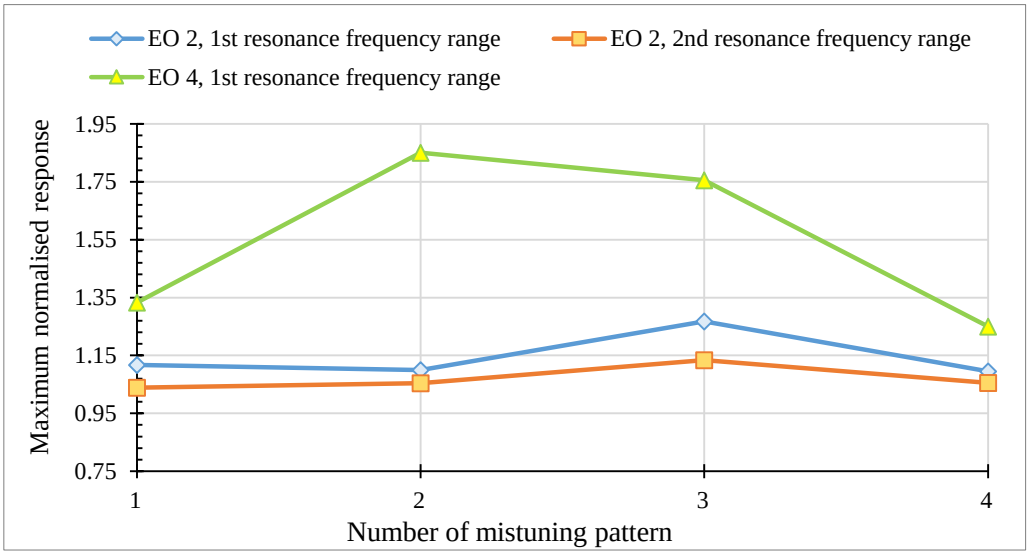

Figure 68: Maximum amplification factors over all the blades for different mistuning pattern

Chapter 5

Conclusions

The key intention of this study is a comprehensive investigation and analysis of the influence of the material anisotropic orientations on the dynamic properties of a gas turbine bladed disc with monocrystalline anisotropic blades. Therefore, three finite element models were created : (a) a single blade finite element model to analyse the effects of material anisotropy on the modal properties of a single blade of a gas turbine, (b) a finite element sector model with cyclic symmetry to analyse the influence of anisotropic material orientations on the natural frequency and mode shapes of a tuned bladed disc, and (c) a whole bladed disc finite element model (tuned and mistuned) to investigate the effects of anisotropic material orientations on the forced responses of a mistuned bladed disc of a gas turbine. Harmonic forced responses of the tuned and mistuned bladed disc were calculated using mode superposition method. For these analyses, nickel-based superalloy DZ125 was chosen as a material for monocrystalline anisotropic gas turbine blades. Finally, 2D and 3D response charts are plotted for different cases to analyse the variation of the natural frequency of a single blade and a tuned bladed disc respectively due to the variation of anisotropic material orientations of the blade material. Also, normalised forced responses of the mistuned bladed disc with four different mistuning patterns are plotted against a number of blades of the whole bladed disc.

From this entire study, the following conclusions and recommendations were made-

i) Material anisotropy has a significant effect on the dynamic properties of a gas turbine bladed disc with monocrystalline anisotropic blades.

ii) In the case of a single blade, maximum frequency variation due to material anisotropy is found to be 5.3 % amongst the investigated cases.

iii) For tuned bladed disc, maximum frequency variation is found to be 5.1 % amongst the examined cases.

iv) Frequency values are found to be maximum in most of the analysed cases when secondary angle (ψ) is equal to 80°, [see Figure 23, Figure 24, Figure 25 to Figure 27, Figure 39 to Figure 48].

v) Frequency values are found to be minimum in most of the investigated cases when secondary angle (ψ) is somewhere in between 20° to 30° ($\psi \cong 25°$), [see Figure 23, Figure 25 to Figure 27, Figure 39 to Figure 48].

vi) Frequency values are found to be minimum in most of the investigated cases when values of primary angles are either ($\varphi = -15°$, $\theta = -15°$) or ($\varphi = 15°$, $\theta = 15°$), [see Figure 22, Figure 24, Figure 28 to Figure 30, Figure 34 to Figure 38].

vii) Amplification factor or normalised maximum forced responses are found to be within the range of 0.66 to 1.85 for the investigated cases of mistuned bladed disc with four different mistuning patterns of the monocrystalline anisotropic blade material.

References

[1] Nair, S., Nair, S., Chhabra, T., Verma, P., Mittal, S., (2014) *Steady state structural analysis of high pressure gas turbine blade*, International Journal of Engineering Research & Technology, 3(5), pp. 980-985, ISSN: 2278-0181

[2] Hu, X., Yang, X., Shi, D., Yu, H., and Ren, T., (2016), *Constitutive modeling of a directionally solidified nickel-based superalloy DZ125 subjected to thermal mechanical creep fatigue loadings*, pp 1-15, Available at : http://link.springer.com/article/10.1007/s12598-016-0713-8/fulltext.html [Accessed on: 7th June 2016]

[3] Rao J. S., (2006) *Mistuning of bladed disc assemblies to mitigate resonance*, Advances in Vibration Engineering, Krishtel Emaging Solutions Private Limited, Available at: http://www.altairhyperworks.co.uk/html/en-GB/PD_Datasheets/APD_Mitigating%20 Resonance.Pdf

[4] James, B. M., (2004), *Reduced-order blade mistuning analysis techniques developed for the robust design of engine rotors*, NASA Glenn Research Center, Research and Technology; (NASA/TM-2004-212729), Available at: http://ntrs.nasa.gov/archive/nasa/casi.ntrs.nasa.gov/ 20050215271.pdf

[5] Choi, Y. S., Gottfried, D.A., and Fleeter, S., (2004) *Analysis of structural mistuning effects on bladed disc vibrations including aerodynamic damping*, International Compressor Engineering Conference, School of Mechanical Engineering, Purdue University, C140, pp. 1-7.

[6] Sinha, A., and Chen, S. (1989), *A higher order technique to compute the statistics of forced response of a mistuned bladed disc assembly*, Journal of Sound and Vibration, M(2), 207-221

[7] Petrov, E.P., Ewins, D.J., (2003), *Analysis of the worst mistuning patterns in bladed disc Assemblies, Journal of Turbomachinery*, Vol. 125, ASME, pp. 623-631.

[8] Rahimi, M., and Ziaei-Rad, S., (2009) *Uncertainty treatment in forced response calculation of mistuned bladed disc*, Mathematics and Computers in Simulation 80 (2010) 1746–1757

[9] Kaza, Krishna R.V. and Kielb, R.E., (1984) *Vibration and flutter of mistuned bladed-disc assemblies*, Twenty-fifth Structures, Structural Dynamics and Material Conference, Palm Springs, California, NASA Technical Memorandum 83634, AIAA-84-0991, pp. 1-18.

[10] Petrov, E., Sanliturk, K., Ewins, D., and Elliott, R., *Quantitative prediction of the effects of mistuning arrangement on resonant response of a practical turbine bladed disc,* Imperial College of Science, Rolls-Royce Plc, UK

[11] Castanier, M.P., Pierre, C., (2006) *Modeling and analysis of mistuned bladed disc vibration: status and emerging directions, Journal of Propulsion and Power, 22(2), pp. 384-396,*

[12] Stefanescu, D. (2008), *Science and Engineering of Casting Solidification*, Second Edition, Springer Science & Business Media.

[13] What is Directional Solidification? - Magic Marks. (2014). [video] Magic Marks, India. Available at: https://www.youtube.com/watch?v=8xVDy8OzeKc, [Accessed on: 1st May 2016]

[14] Slideshare.net. (2016). Ch11 casting process Erdi Karaçal Mechanical Engineer University of Gaziantep [online] Available at: http://www.slideshare.net/garacaloglu/ch11-casting-process [Accessed 20 Aug. 2016].

[15] Dinçkal, Ç. (2012). *On the properties of anisotropic engineering materials based upon orthonormal representations,* International Journal of Applied Mathematics, 42(3).

[16] www.autofemsoft.com, (2016). Anisotropic Materials[online] Available at: http://www.autofemsoft.com/help/anisotropic_materials.html [Accessed 20 Aug. 2016].

[17] Efunda.com. (2016). Hooke's Law for Orthotropic Materials. [online] Available at: http://www.efunda.com/formulae/solid_mechanics/mat_mechanics/hooke_orthotropic.cfm [Accessed 20 Aug. 2016].

[18] Savage, M.W.R.,(2011), *The influence of crystal orientation on the elastic stresses of a single crystal nickel-based turbine blade,* Proceedings of ASME Turbo Expo, GT2011-45309, Vancouver, British Columbia, Canada

[19] Wen, Z., Mao, H., Yue, Z. and Wang, B. (2013) *The influence of crystal orientation on vibration characteristics of DD6 nickel-base single crystal superalloy turbine blade,* Journal of Materials Engineering and Performance, 23(2), pp. 372-377.

[20] Swanson, G.R., Arakere, N.K., (2000), Effect of crystal orientation on analysis of single-crystal, nickel-based turbine blade superalloys, NASA / TP--2000-210074, Marshall Space Flight Center.

[21] Petrov, Y (2016), Finite Element Analysis, Available from: https://studydirect.sussex.ac.uk/ course/ view.php?id=24454&topic=1, [Accessed: 25th February, 2016]

[22] Introduction in finite element analysis with ANSYS, Available from: https://studydirect. sussex.ac.uk/course/view.php?id=24454&topic=1, [Accessed: 25th February, 2016]

[23] Petrov, Y. (2016). Study Direct, Modal analysis. [online] Studydirect.sussex.ac.uk. Available at: https://studydirect.sussex.ac.uk/course/view.php?id=24454&topic=7 [Accessed 20 Aug. 2016].

[24] Petrov, E. (2016). Study Direct, Harmonic Analysis. [online] Studydirect.sussex.ac.uk. Available at: https://studydirect.sussex.ac.uk/course/view.php?id=24454&topic=8 [Accessed 20 Aug. 2016].

[25] ANSYS (2016). Harmonic Analysis, Chapter Ten, [online] Available at: http://www-eng.lbl.gov/~als/FEA/ANSYS_V9...9.0.../AWS90_Ch10_Harmonic.ppt [Accessed 20 Aug. 2016].

[26] R.Z. Chen, Development Status of Single Crystal Superalloys, J. Mater. Eng., 1995, 8, p 3–12

[27] A. Scholz, A. Schmidt, H. Christian Walther, M. Schein, and M. Schwienheer, (2008) *Experiences in the Determination of TMF, LCF and Creep Life of CMSX-4 in Four-Point Bending Experiments*, Int. J. Fatigue, 30, p 357–362

[28] Q.M. Yu, Z.F. Yue, and Z.X. Wen, (2008) *Creep Damage Evolution in a Modeling Specimen of Nickel-Based Single Crystal Superalloys Air-Cooled Blades*, Mater. Sci. Eng., A, 477, p 319–327

[29] N.X. Hou, W.X. Gou, Z.X. Wen, and Z.F. Yue, (2008) *The Influence of Crystal Orientations on Fatigue Life of Single Crystal Cooled Turbine Blad*e, Mater. Sci. Eng., A, 492, p 413–418

[30] N.K. Arakere and G.R. Swanson, (2002) *Effect of Crystal Orientation on Fatigue Failure of Single Crystal Nickel Base Turbine Blade Superalloys*, ASME J. Gas Turbines Power, 2002, 124, p 161–176

[31] Kaneko, Y. et al. (2015) *Resonant response and random response analysis of mistuned bladed disc with directionally solidified blade*, Proceedings of ASME Turbo Expo 2015, Turbine Technical Conference and Exposition, Montreal, Canada, pp. 1-11

[32] Fang, Y., and Li, Y., (2012), *Dynamic responses of nickel-based single crystal superalloy DD6 blade*, Journal of Materials Engineering and Performance, 22(6), pp. 1565–1573.

[33] Kaneko, Y. (2011) *Study on vibration characteristics of single crystal blade and directionally solidified blade,* Proceedings of ASME Turbo Expo, 2009, GT2011, Vancouver, Brotish Columbia, Canada, pp. 1–9

[34] M. Manetti, I. Giovannett, N. Pieroni, Ho. Horculescu et al., *The Dynamic Influence of Crystal Orientation on a Second Generation Single Crystal Material for Turbine Buckets*. Proceedings of ASME Turbo Expo, 2009, GT2009-59180, pp. 1–10

[35] T. Hasebe and M. Sakane, (1994) *Vibration of Nickel-Base Single Crystal and Directionally Solidified Superalloy Plates*, JSME Int J., Ser. A, 37(4), p 481–487

[36] Y, Kanko. (2011) *Study on Vibration Characteristics of Single Crystal Blade and Directionally Solidified Blade*. Proceedings of ASME Turbo Expo, GT2011-45032, pp. 1–10

[37] Kim, T., Hansen, M., A., and Branner, K., (2013) *Development of an anisotropic beam finite element for composite wind turbine blades in multibody system,* Renewable Energy, Vol. 59 pp. 172-183.

[38] Pohle1, L., Scheidt, L. P., and Wallaschek, J. (2015) *Harmonic Mistuning of Blisks,* Section 20: Dynamics and control, pp 641-642, Proceedings in Applied Mathematics and Mechanics, DOI 10.1002/pamm.201510310

[39] Strnad, J., and Liska, J., (2015) *Diagnostic methods of a bladed disc mode shape evaluation used for shrouded blades in steam turbines,* Journal of Physics: Conference Series 659 (2015) 012051, 12th European Workshop on Advanced Control and Diagnosis, IOP Publishing.

[40] Vishwanatha, R.H., Zameer, S., Haneef, M. (2014) *Finite element structural integrity analysis of first stage gas turbine rotor blade assembly under thermo- mechanical loads,* International Journal of Innovative Research in Science, Engineering and Technology, 3 (10), pp. 16433-16441, ISSN 2319-8753

[41] Babu1, J. S., Venkata, A.K.G., Kumar, B.S.P., (2013) *Dynamic response predictions of tuned and mistuned bladed discs using finite element method,* International Journal of Engineering Research & Technology, 2(9), pp. 2752-2755, ISSN: 2278-0181

[42] Kaneko, Y., Ohta, M., Mori, K., and Ohyama, H., (2012), *Study on vibration response reduction of bladed disc by use of asymmetric vane spacing (study on response reduction of mistuned bladed disc),* International Journal of Gas Turbine, Propulsion and Power Systems, 4(1), pp. 35-42.

[43] Nikolic, M., Petrov, E.P., and Ewins, D.J., (2008) *Robust Strategies for Forced Response Reduction of Bladed Disks Based on Large Mistuning Concept,* Journal of Engineering for Gas Turbines and Power, Vol. 130, pp 022501 (1-11), DOI: 10.1115/1.2799524

[44] Yana, Y.J., Cuia, P.L. and Haob, H.N., (2008) *Vibration mechanism of a mistuned bladed-disc,* Journal of Sound and Vibration, 317, pp. 294–307.

[45] Martel, C., and Corral, R., (2008) *Asymptotic description of maximum mistuning amplification of bladed disk forced response*. Proceedings of ASME Turbo Expo 2008: Power for Land, Sea and Air, GT2008, Berlin, Germany.

[46] Nikolic, M., Petrov, E. P., and Ewins, D.J., (2007) *Coriolis forces in forced response analysis of mistuned bladed discs,* Journal of Turbomachinery, Vol. 129, *ASME, pp. 730-739.*

[47] He, z. and Epureanu, B. (2007). Fluid-Structural Coupling Effects on the Dynamics of Mistuned Bladed Disks (AIAA). AIAA Journal, [online] 45(3), pp.552-561. Available at: http://arc.aiaa.org/doi/abs/10.2514/1.23809?journalCode=aiaaj [Accessed 21 Aug. 2016].

[48] Petrov, E.P., and Ewins, D.J., (2005) *Method for Analysis of Nonlinear Multiharmonic Vibrations of Mistuned Bladed Disks With Scatter of Contact Interface Characteristics,* Transactions of the ASME, Vol. 127, pp 127-136, DOI: 10.1115/1.1812781

[49] Petrov, E.P., and Ewins, D.J., (2003) Analysis of the Worst Mistuning Patterns in Bladed Disk Assemblies, Journal of Turbomachinery, Vol. 125, pp 623-631, DOI: 10.1115/1.1622710

[50] Petrov, E.P., Sanliturk, K.Y., Ewins, D.J., (2002) *A new method for dynamic analysis of mistuned bladed disks based on the exact relationship between tuned and mistuned systems,* Transactions of the ASME, Vol. 124, pp 586-597, DOI: 10.1115/1.1451753

[51] Moyroud, F., and Fransson, T., (2002) *A comparison of two finite element reduction techniques for mistuned bladed discs, Journal of Turbomachinery, Vol. 124, ASME, pp. 942-952.*

[52] Yang, M.T., and Griffin, J.H., (1999), *A reduced order model of mistuning using a subset of nominal system modes,* The American society of mechanical engineers, International Gas Turbine &

Aeroengine Congress & Exhibition, Indianapolis, Indiana, Available at : http://proceedings.asmedigitalcollection.asme.org/

[53] Web.mit.edu. (2016). Ten-node tetrahedral element (C3D10 and F3D10). [online] Available at: http://web.mit.edu/calculix_v2.7/CalculiX/ccx_2.7/doc/ccx/node33.html [Accessed 20 Aug. 2016].

[54] www.colorado.edu. (2016). The Quadratic Tetrahedron, University of Colorado Boulder [online] Available at: http://www.colorado.edu/engineering/CAS/courses.d/AFEM.d/AFEM.Ch10.d/AFEM .Ch10.pdf [Accessed 20 Aug. 2016].

[55] Web.mit.edu. (2016). Twenty-node brick element (C3D20 and F3D20). [online] Available at: http://web.mit.edu/calculix_v2.7/CalculiX/ccx_2.7/doc/ccx/node29.html [Accessed 20 Aug. 2016].

[56] www.colorado.edu. (2016). Hexahedron Elements, University of Colorado Boulder. [online] Available at: http://www.colorado.edu/engineering/CAS/courses.d/AFEM.d/AFEM.Ch11.d/ AFEM.Ch11.pdf [Accessed 20 Aug. 2016].

[57] www.specialmetals.com. (2016). Special Metals. [online] Available at: http://www. specialmetals. com/assets/documents/alloys/inconel/inconel-alloy-706.pdf [Accessed 30 Aug. 2016].

[58] Fernandobatista.net. (2016). ANSYS Customer Portal - ANSYS 12.0 Tutorials. [online] Available at: http://fernandobatista.net/education/project/Ansys12/Tutorials/ [Accessed 21 Aug. 2016].

[59] Using Design Xplorer 12.0. (2009). ANSYS, Inc. Proprietary, Chapter 2 (Inventory #002670), pp.2-1 to 2-33.